Supplementary Information

Prediction of Trace Organic Contaminant Abatement with UV/H_2O_2: Development and Validation of Semi-Empirical Models for Municipal Wastewater Effluents

DANIEL GERRITY[1,2,3]*, YUNHO LEE[4,5+], SUJANIE GAMAGE[3,6], MINJU LEE[5,7], ALEKSEY N. PISARENKO[2,3], REBECCA A. TRENHOLM[3], URS VON GUNTEN[5,7], AND SHANE A. SNYDER[8]

[1]*Department of Civil and Environmental Engineering, University of Nevada, Las Vegas, Box 454015, 4505 S. Maryland Parkway, Las Vegas, NV 89154-4015, United States*

[2]*Trussell Technologies, Inc., 6540 Lusk Blvd., Suite C274, San Diego, CA 92121, United States*

[3]*Applied Research and Development Center, Southern Nevada Water Authority, P.O. Box 99954, Las Vegas, NV 89193-9954, United States*

[4]*School of Environmental Science and Engineering, Gwangju Institute of Science and Technology, 123, Oryong-dong, Buk-gu, Gwangju 500-712, Korea*

[5]*Eawag, Swiss Federal Institute of Aquatic Science and Technology (Eawag), Ueberlandstrasse 133, P.O. Box 611, 8600 Duebendorf, Switzerland*

[6]*Clark County Water Reclamation District, 5857 E. Flamingo Rd., Las Vegas, NV 89122, United States*

[7]*School of Architecture, Civil, and Environmental Engineering (ENAC), Ecole Polytechnique Federale de Lausanne, CH-1015, Lausanne, Switzerland*

[8]*Department of Chemical and Environmental Engineering, University of Arizona, 1133 E. James E. Rogers Way, Harshbarger 108, Tucson, AZ 85721-0011, United States*

*Corresponding author. Mailing address: Department of Civil and Environmental Engineering, University of Nevada, Las Vegas, Box 454015, 4505 S. Maryland Parkway, Las Vegas, NV 89154-4015, United States. Phone: (702) 895-3955. Fax: (702) 895-3936. Email: Daniel.Gerrity@unlv.edu.

+Corresponding author. Mailing address: School of Environmental Science and Engineering, Gwangju Institute of Science and Technology, 123, Oryong-dong, Buk-gu, Gwangju 500-712, Korea. Phone: (82) 62 715 2468. Fax: (82) 62 715 2434. Email: yhlee42@gist.ac.kr.

Text S1. Description of analytical methods.

Online SPE and LC-MS/MS for TOrC Quantification. *The following is adapted from Snyder et al. (2014) and Lee et al. (2013).* Except for atrazine, which was purchased from ChemService (West Chester, PA, USA), the target TOrCs were obtained from Sigma-Aldrich (St. Louis, MO, USA). Isotopically labeled compounds were obtained from Toronto Research Chemicals (Ontario, Canada), C/D/N Isotopes (Pointe-Claire, Canada), or Cambridge Isotope Laboratories (Andover, MA, USA). All concentrated stock solutions were prepared in methanol and stored at -20°C. Working stock solutions were prepared frequently in either reagent water or methanol and stored at 4°C. All solvents were trace analysis grade from Burdick and Jackson (Muskegon, MI). Reagent water was obtained using a Milli-Q Ultrapure Water Purification System (Millipore, Bedford, MA, USA).

The TOrCs were analyzed by on-line solid phase extraction (SPE) followed by liquid chromatography tandem mass spectrometry (LC-MS/MS) with isotope dilution (Trenholm et al., 2009). This method was selected due to reduced sample volumes, solvent volumes, and total analysis time per sample (~20 minutes) compared to traditional off-line SPE-LC-MS/MS methods. Therefore, this method was able to shorten sample turn-around times and increase experimental throughput. On-line SPE-LC-MS/MS was accomplished with a Symbiosis Pharma (Spark Holland, Emmen, the Netherlands) system in XLC mode using Analyst® 1.4.2 (Applied Biosystems, Foster City, CA). Samples were collected in 40-mL amber glass vials with a quenching agent (50 mg/L ascorbic acid) and preservative (1 g/L sodium azide). If analysis was not performed immediately following each experiment, samples were refrigerated at 4°C and extracted within 14 days of collection. Prior to analysis, 10 mL of sample was measured in a volumetric flask and spiked with isotopically-labeled standards at 100 ng/L. This provided

sufficient sample volume for replicates, matrix spikes, and dilutions, if necessary. A 1.5-mL aliquot of each sample was transferred into a 2-mL autosampler vial, although only 1.0 mL was used for extractions. Extractions were performed using Waters Oasis HLB Prospekt cartridges (30 mm, 2.5 mg, 10 x 1 mm, 96 tray) (Milford, MA). Prior to sample loading, each cartridge was sequentially conditioned with 1 mL of dichloromethane (DCM), methyl tert-butyl ether (MTBE), methanol, and reagent water (Milli-Q). Samples were loaded onto the SPE cartridges at 1 mL/min after which the cartridges were washed with 1 mL of reagent water. After sample loading, the analytes were eluted from the SPE cartridge to the LC column with 200 mL methanol, using the LC peak focusing mode. A 5-mM ammonium acetate solution and methanol gradient was used for LC mobile phases with a flow rate of 800 mL/min. Analytes were separated using a 150 x 4.6-mm Luna C18(2) column with a 5-µm particle size (Phenomenex, Torrance, CA).

Method reporting limits (MRLs) were established at 3 to 5 times the calculated method detection limits (MDLs). The MRLs for the target compounds are listed in Table 2 in the main text. Although lower MRLs can be achieved with off-line SPE-LC-MS/MS methods, the elevated concentrations in wastewater, particularly after spiking at 1 µg/L, were sufficient to justify the use of the on-line alternative. Stringent QA/QC protocols (i.e. matrix spikes, duplicate samples, field blanks, and laboratory blanks) were followed throughout the duration of the project. Based on extensive method development and past studies, the concentrations of duplicate samples rarely varied by greater than 5%. Additional details are provided in Trenholm et al. (2009).

Automated SPE and GC-MS/MS for NDMA Analysis. *The following is adapted from Gerrity et al. (2015).* NDMA analysis was performed with isotope dilution using a modified

version of United States (U.S.) Environmental Protection Agency (EPA) method 521 (Holady et al., 2012). Trace analysis grade methanol and DCM were obtained from Burdick and Jackson (Muskegon, MI, USA). NDMA standards were purchased from Ultra Scientific (Kingstown, RI, USA), and isotopically labeled NDMA was purchased from Cambridge Isotope Laboratories (Andover, MA, USA). Working stock solutions of NDMA and isotopically labeled NDMA were made in DCM. Appropriate dilutions were made in methanol for automated SPE spiking solutions (i.e., NDMA spike mix and isotopically labeled standards). Calibration standards (minimum of seven ranging from 1.0 to 500 µg/L) were made in DCM and were replaced every three months. All stock solutions, automated SPE spiking solutions, and calibration standards were stored at -20 °C.

Automated (SPE) was performed using a Dionex AutoTrace workstation (Thermo Scientific, Sunnyvale, CA, USA). Samples were spiked with 100 µL of isotope mix at 0.5-2.5 mg/L for a final concentration of 100-500 µg/L in the final extract. Pre-packed activated carbon cartridges (Resprep 521, Restek, Bellefonte, PA, USA) were sequentially conditioned with 5 mL of DCM, 5 mL of methanol, and 10 mL of reagent grade water with flow rates of 15 mL/min. Samples were loaded at a rate of 15 mL/min. Cartridges were rinsed with 5 mL of reagent grade water with a flow rate of 20 mL/min and dried for 10 min with nitrogen gas. Analytes were eluted with 10 mL of DCM into 15 mL conical vials (Dionex) with a flow rate of 5 mL/min. Extracts were evaporated under nitrogen gas to approximately 2 mL. Water was then removed from the DCM extracts by passing the 2 mL extract through a DryDisk separation membrane (Horizon Technology, Salem, NH, USA). The DCM extract was collected and concentrated to a final volume of 500 µL with nitrogen gas, resulting in a 1:2000 concentration factor.

A Varian (Walnut Creek, CA) CP-3800 Gas Chromatograph with a CP-8400 auto

sampler was used for all analyses. The injector (Varian 1177) was operated in splitless mode with a Siltek deactivated glass liner (Restek, Bellefonte, PA) and set at a temperature of 200°C. Analytes were separated on a 30 m x 0.32 mm ID x 1.4 µm DB624 column (J & W, Agilent, Palo Alto, CA) using a 1.4 mL/min helium flow with an initial pressure pulse of 35 psi for 0.85 min. The temperature program was as follows: 35°C, hold for 1.0 min; 35-120°C at 5°C/min; 120-145°C at 3°C/min; 145-250°C at 35°C/min, hold for 4.64 min. An injection volume of 2 µL was used for all analyses. The transfer line was set at 240°C.

Analysis was performed using a Varian 4000 ion trap mass spectrometer (Walnut Creek, CA). All analyses were performed using multiple reaction monitoring (MRM) in positive chemical ionization mode using liquid methanol. A summary of NDMA attributes and the precursor and product ions used for quantitation and confirmation is shown below. The MRL of 2.5 ng/L was established at 3 to 5 times the calculated method detection limit (n=12). A laboratory reagent blank was included in each extract batch. Acceptable average percent recoveries were limited to 70-130%, and acceptable relative standard deviations (RSDs) were limited to 30% for replicate samples.

Nitrosamine	CAS#	Structure	Isotope	MW (amu)	Precursor Ion (m/z)	Product Ion (m/z)	MRL (ng/L)
N-nitrosodimethylamine (NDMA)	62-75-9	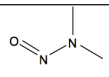	NDMA-d_6	74	75	47 (44, 43, 58) [a]	2.5

[a] ( ) – confirmation product ions

Figure S1. Abatement of NDMA with (A) UV photolysis at 254 nm and (B) UV/H_2O_2 with 10 mg/L of H_2O_2. The secondary effluents are differentiated with symbols, but the linear regression was performed on the combined data sets.

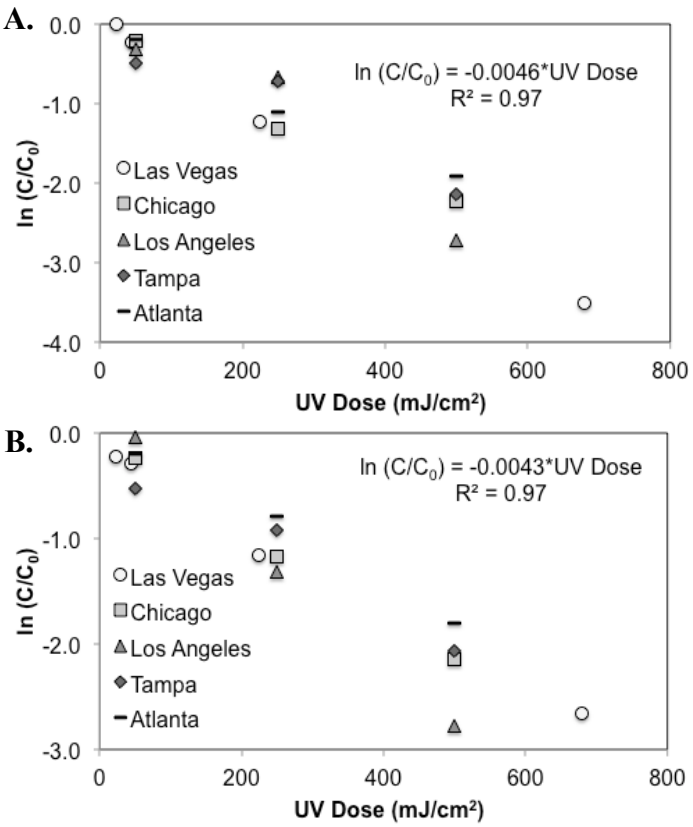

Figure S2. Decadic molar extinction coefficients (ε, M^{-1} cm^{-1}) of the target compounds as a function of wavelength. The ε_{254} for each compound is reported below each figure and also in Table 2 in the main text. Base *e* molar extinction coefficients ($\varepsilon'_{254} = \varepsilon_{254} \times 2.303$) are also provided for reference.

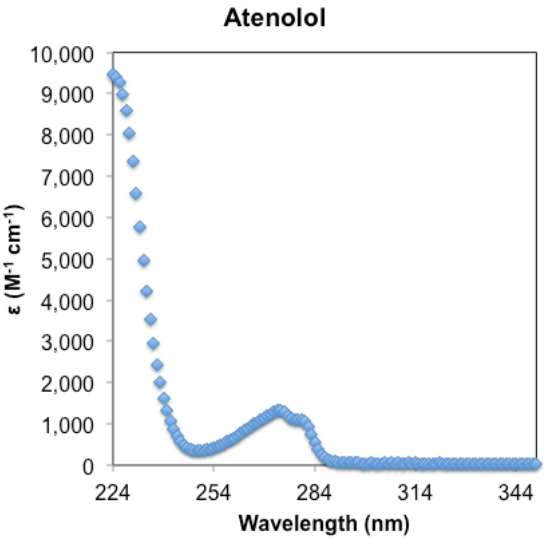

ε_{254} = 425 M^{-1} cm^{-1}
ε'_{254} = 979 M^{-1} cm^{-1}

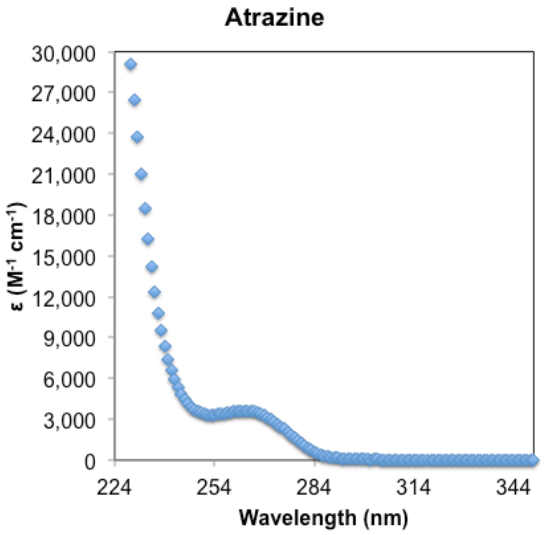

ε_{254} = 3334 M^{-1} cm^{-1}
ε'_{254} = 7678 M^{-1} cm^{-1}

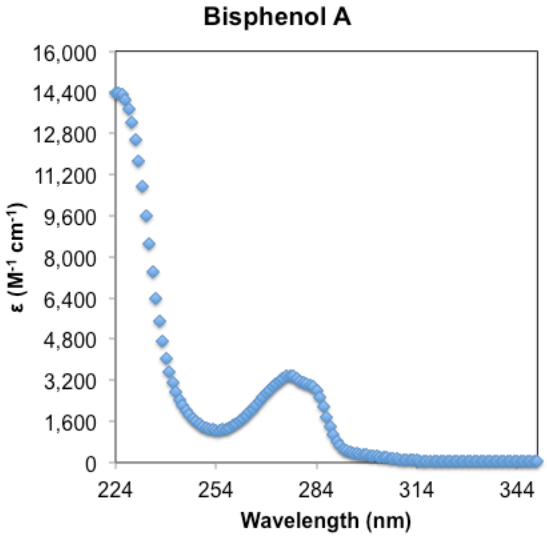

ε_{254} = 1253 M^{-1} cm^{-1}
ε'_{254} = 2886 M^{-1} cm^{-1}

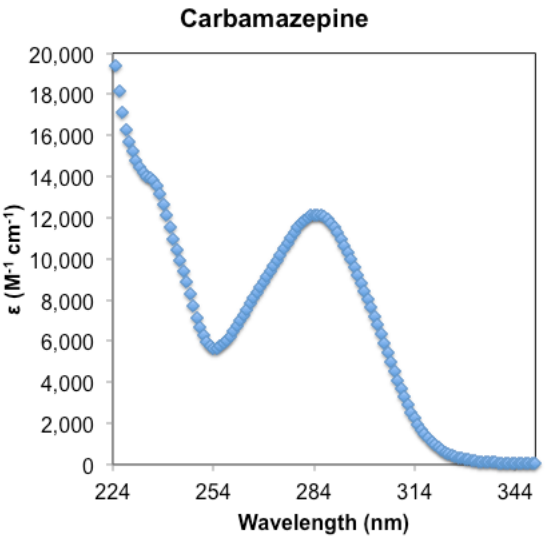

ε_{254} = 5672 M^{-1} cm^{-1}
ε'_{254} = 13063 M^{-1} cm^{-1}

Figure S2 (cont.). Decadic molar extinction coefficients (ε, M^{-1} cm^{-1}) of the target compounds as a function of wavelength. The ε_{254} for each compound is reported below each figure and also in Table 2 in the main text. Base *e* molar extinction coefficients ($\varepsilon'_{254} = \varepsilon_{254}$ x 2.303) are also provided for reference.

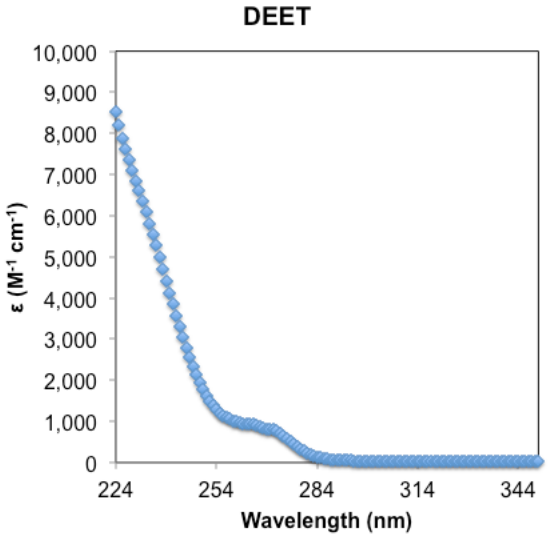

ε_{254} = 1294 M^{-1} cm^{-1}
ε'_{254} = 2980 M^{-1} cm^{-1}

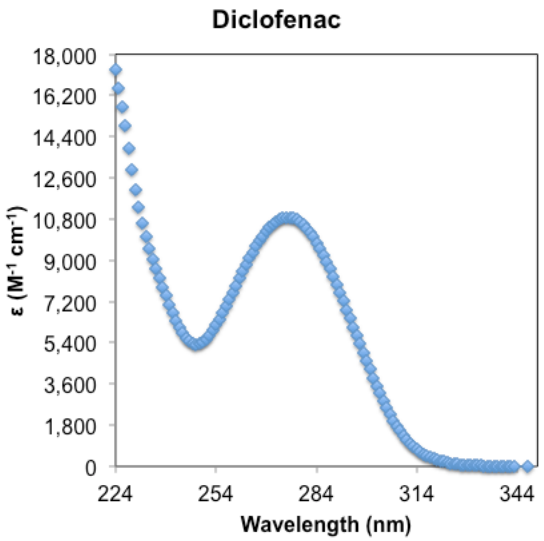

ε_{254} = 6162 M^{-1} cm^{-1}
ε'_{254} = 14191 M^{-1} cm^{-1}

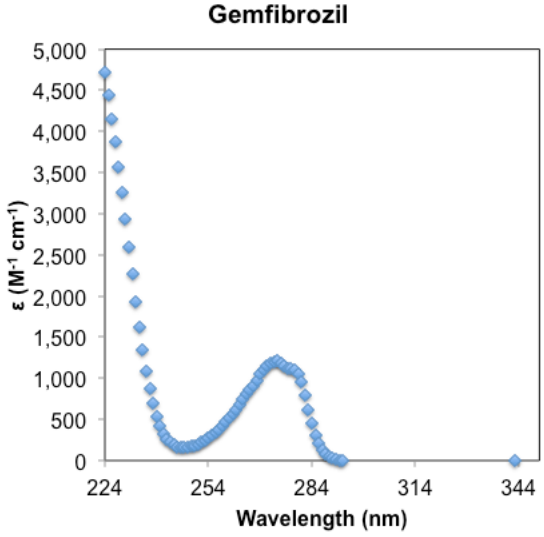

ε_{254} = 269 M^{-1} cm^{-1}
ε'_{254} = 620 M^{-1} cm^{-1}

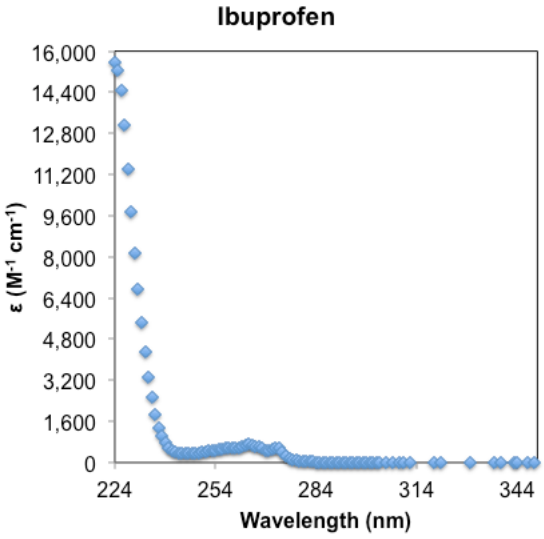

ε_{254} = 471 M^{-1} cm^{-1}
ε'_{254} = 1085 M^{-1} cm^{-1}

Figure S2 (cont.). Decadic molar extinction coefficients (ε, M^{-1} cm^{-1}) of the target compounds as a function of wavelength. The ε_{254} for each compound is reported below each figure and also in Table 2 in the main text. Base *e* molar extinction coefficients ($\varepsilon'_{254} = \varepsilon_{254}$ x 2.303) are also provided for reference.

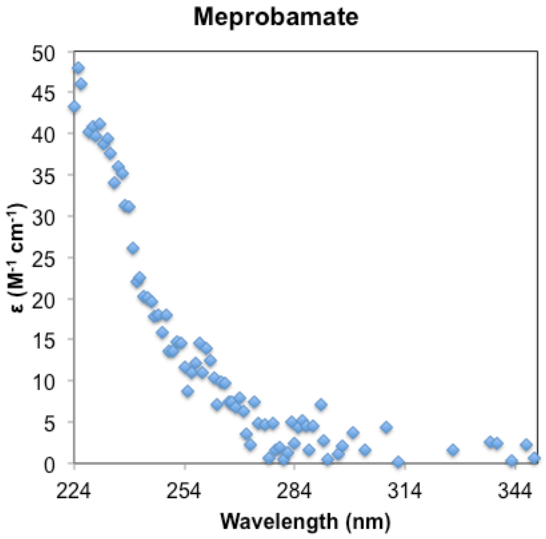

ε_{254} = 12 M^{-1} cm^{-1}
ε'_{254} = 28 M^{-1} cm^{-1}

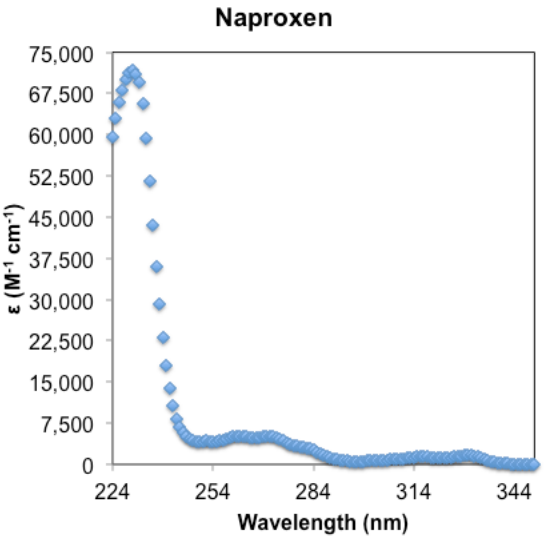

ε_{254} = 4215 M^{-1} cm^{-1}
ε'_{254} = 9707 M^{-1} cm^{-1}

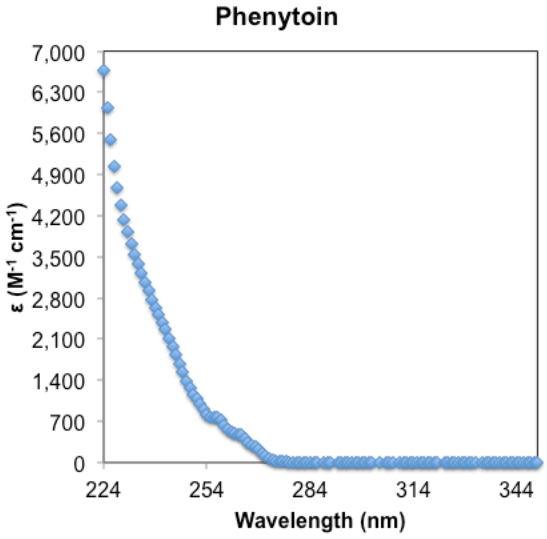

ε_{254} = 813 M^{-1} cm^{-1}
ε'_{254} = 1872 M^{-1} cm^{-1}

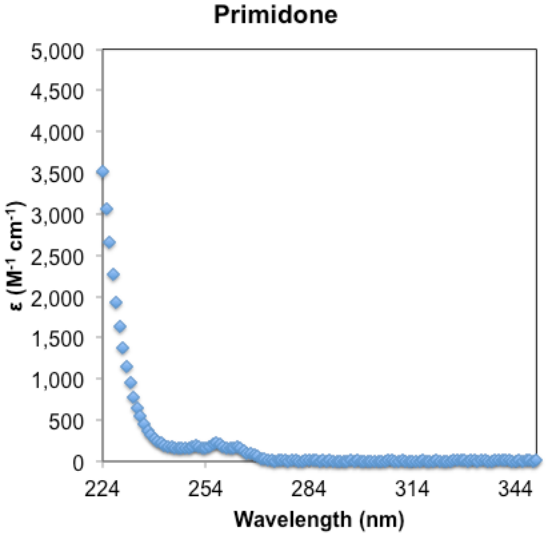

ε_{254} = 168 M^{-1} cm^{-1}
ε'_{254} = 387 M^{-1} cm^{-1}

Figure S2 (cont.). Decadic molar extinction coefficients (ε, M^{-1} cm^{-1}) of the target compounds as a function of wavelength. The ε_{254} for each compound is reported below each figure and also in Table 2 in the main text. Base *e* molar extinction coefficients ($\varepsilon'_{254} = \varepsilon_{254} \times 2.303$) are also provided for reference.

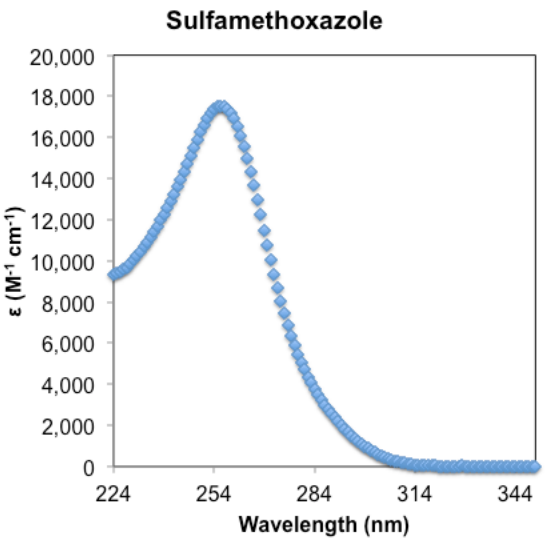

ε_{254} = 17362 M^{-1} cm^{-1}
ε'_{254} = 979 M^{-1} cm^{-1}

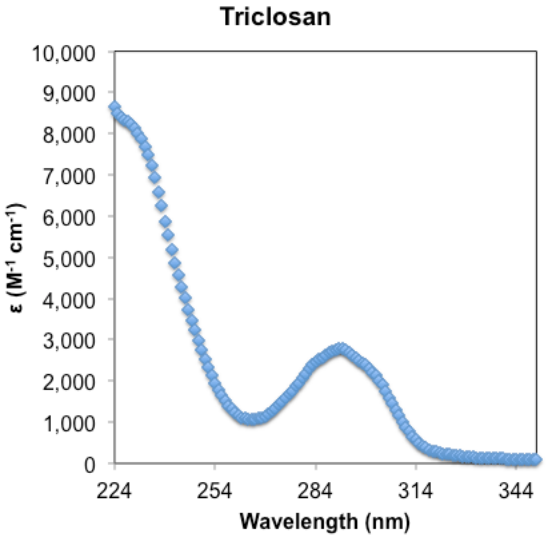

ε_{254} = 1947 M^{-1} cm^{-1}
ε'_{254} = 4484 M^{-1} cm^{-1}

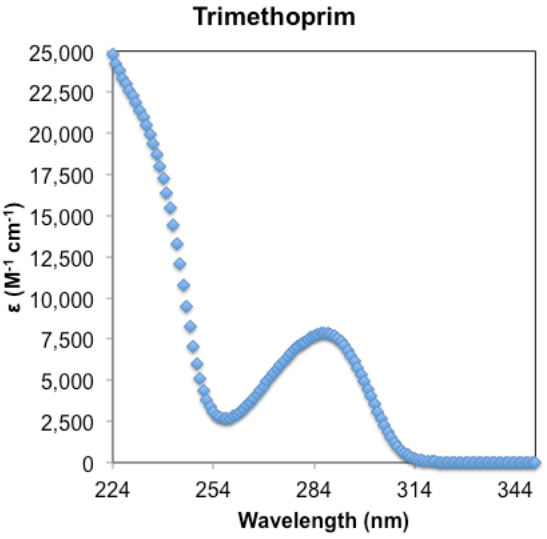

ε_{254} = 3053 M^{-1} cm^{-1}
ε'_{254} = 7031 M^{-1} cm^{-1}

Figure S3A. Determination of $R_{\cdot OH,UV}$ values (5 mg/L of H_2O_2) for the 5 secondary effluents from the U.S. An H_2O_2 dose of 5 mg/L was not tested for the Las Vegas wastewater.

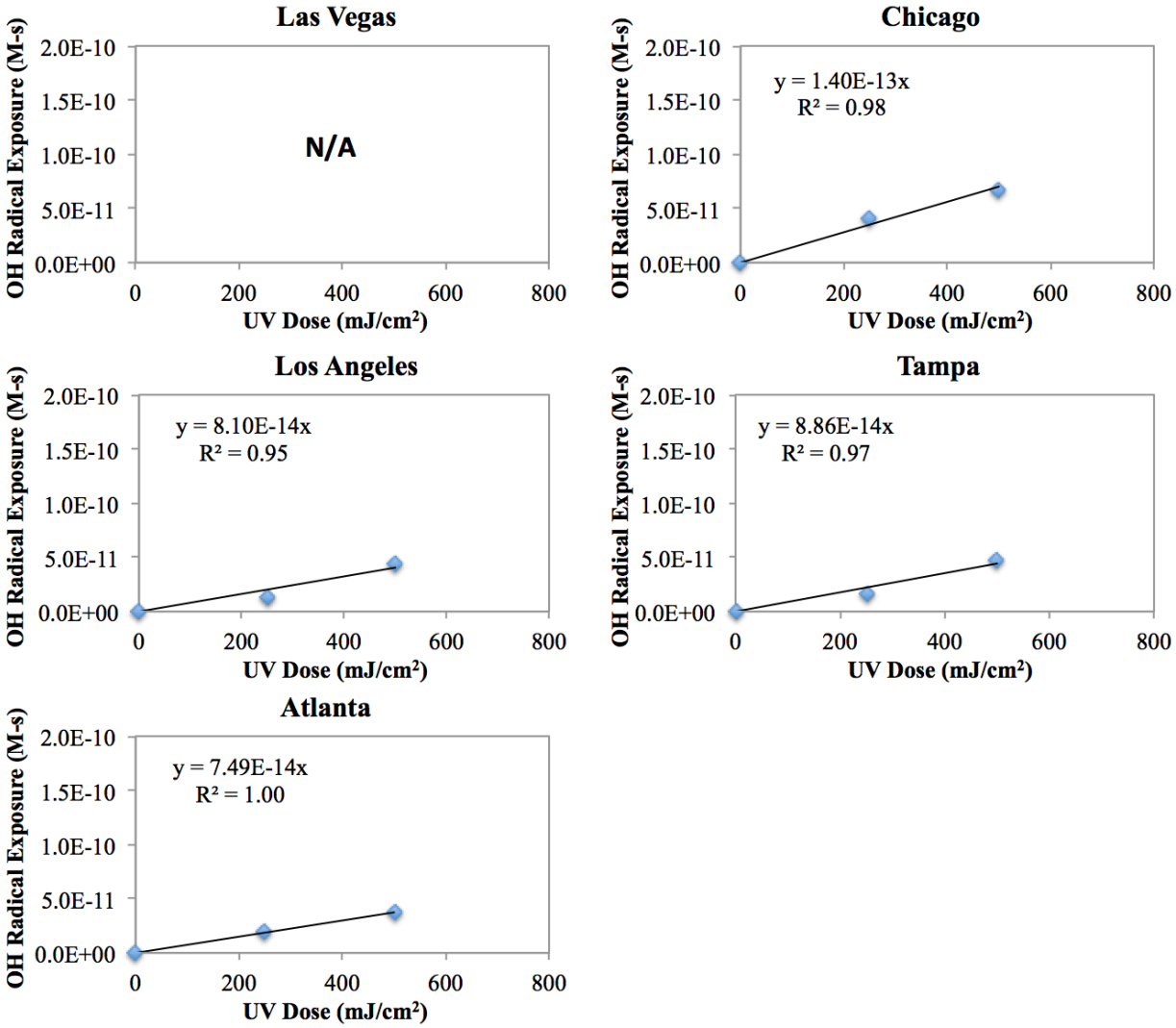

Figure S3B. Determination of $R_{\cdot OH,UV}$ values (10 mg/L of H_2O_2) for the 5 secondary effluents from the U.S.

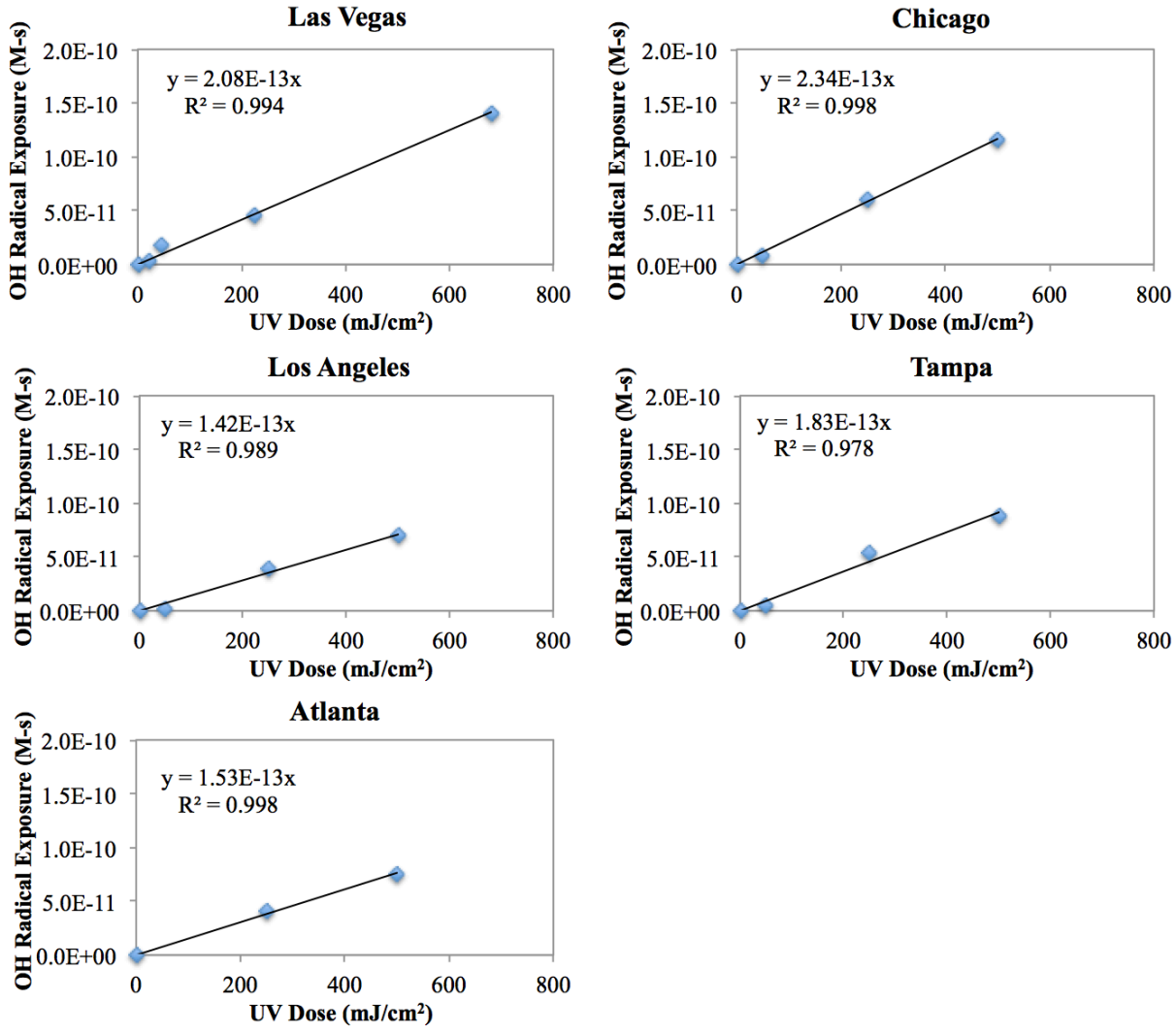

Figure S3C. Determination of $R_{\cdot OH,UV}$ values (10 mg/L of H_2O_2) for the 5 secondary effluents from CH and AUS.

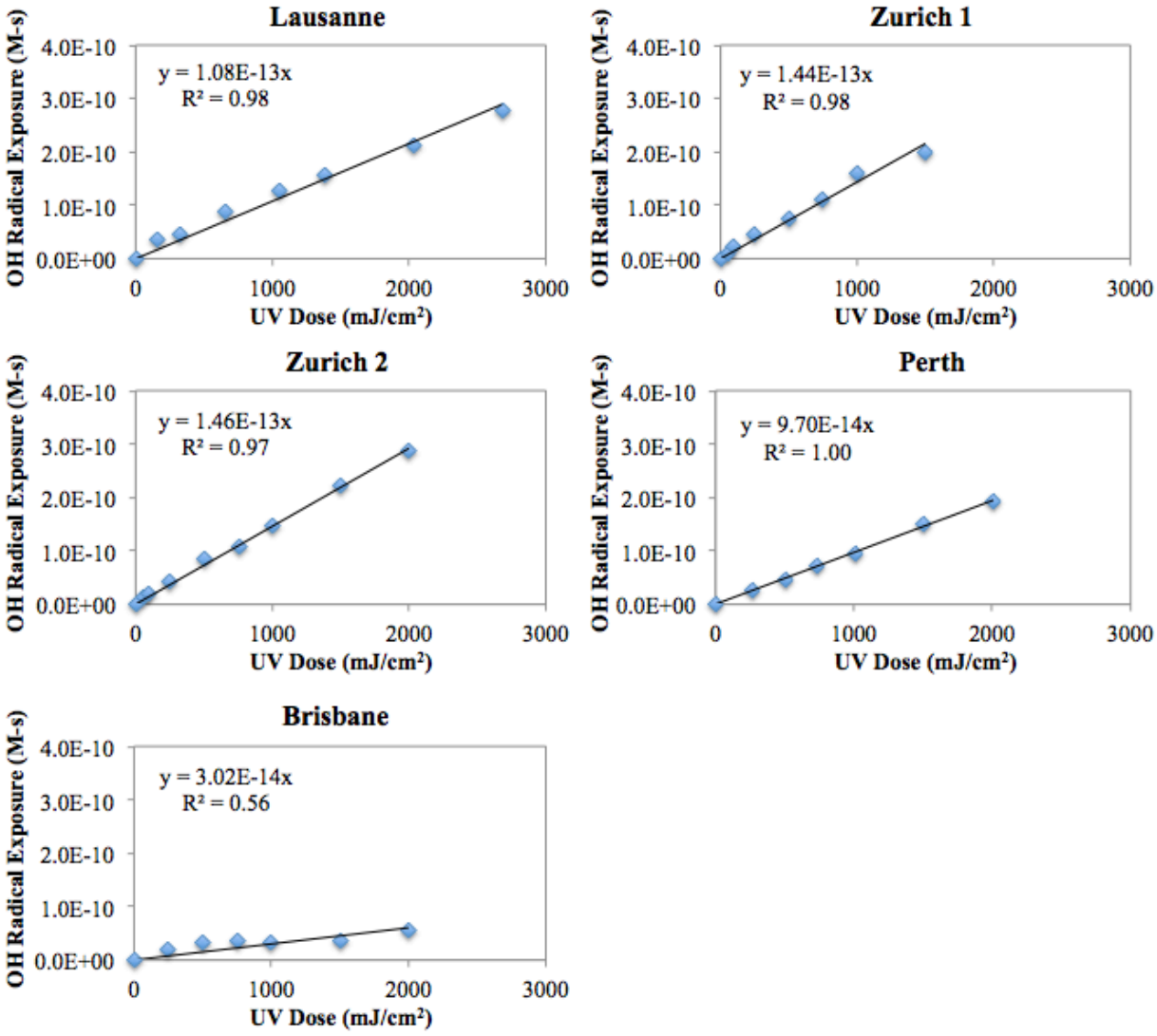

Figure S4A. Abatement of diclofenac with UV and UV/H_2O_2 (10 mg/L of H_2O_2). Abatement levels are reported as a function of UV dose (left) and UV dose normalized to DOC (right).

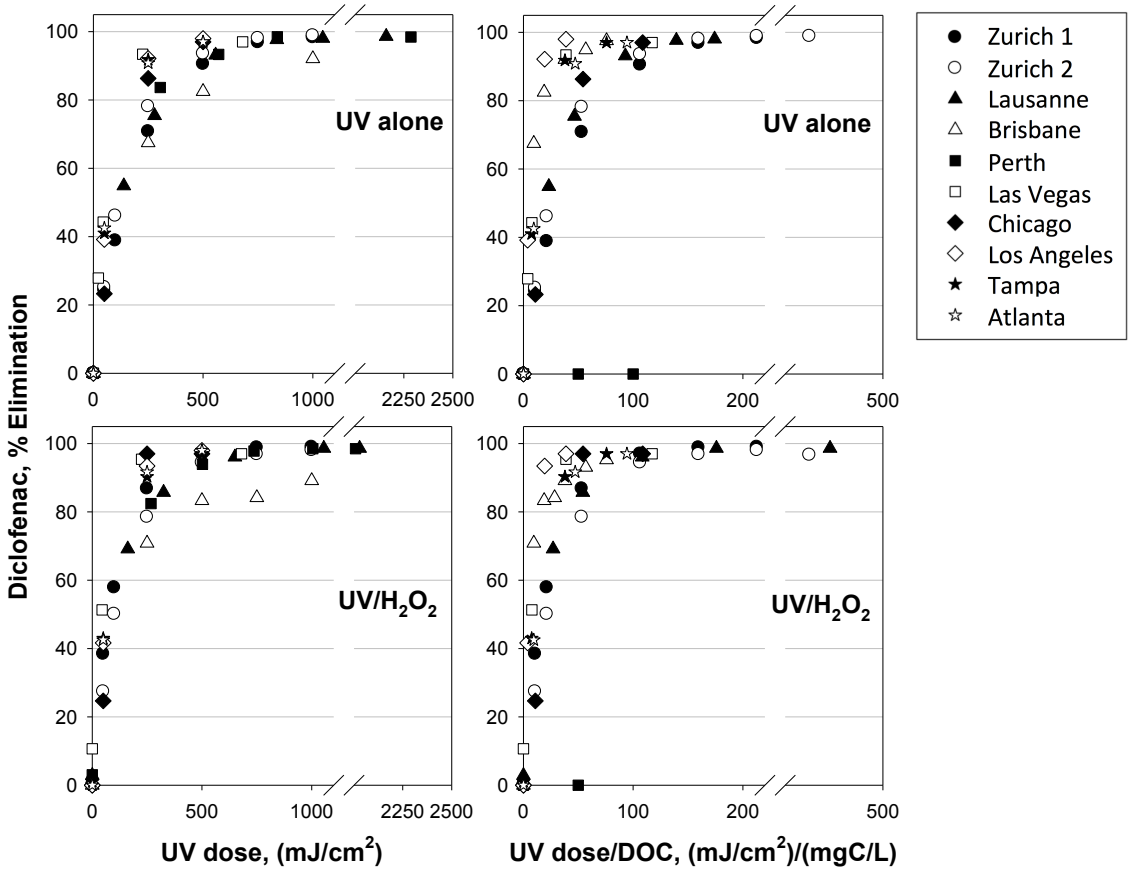

Figure S4B. Abatement of triclosan with UV and UV/H_2O_2 (10 mg/L of H_2O_2). Abatement levels are reported as a function of UV dose (left) and UV dose normalized to DOC.

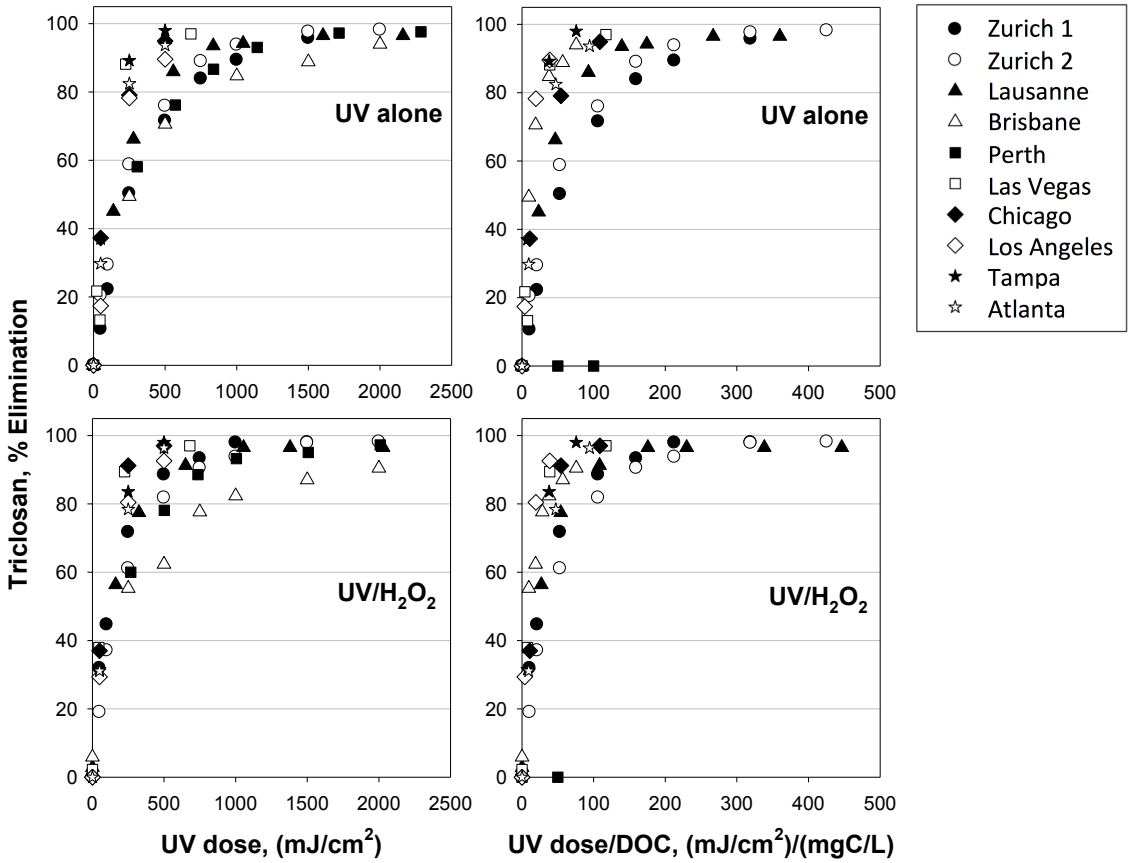

Figure S4C. Abatement of sulfamethoxazole with UV and UV/H_2O_2 (10 mg/L of H_2O_2). Abatement levels are reported as a function of UV dose (left) and UV dose normalized to DOC.

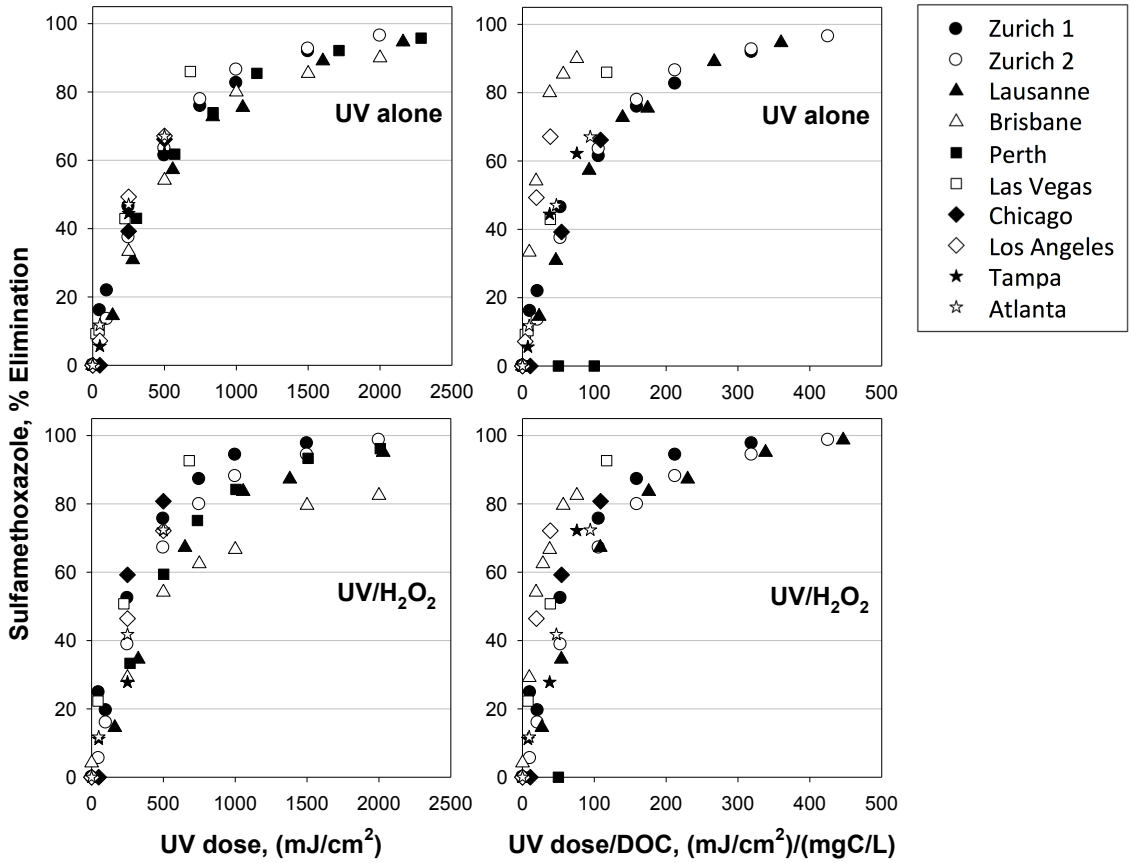

Figure S4D. Abatement of phenytoin with UV and UV/H_2O_2 (10 mg/L of H_2O_2). Abatement levels are reported as a function of UV dose (left) and UV dose normalized to DOC.

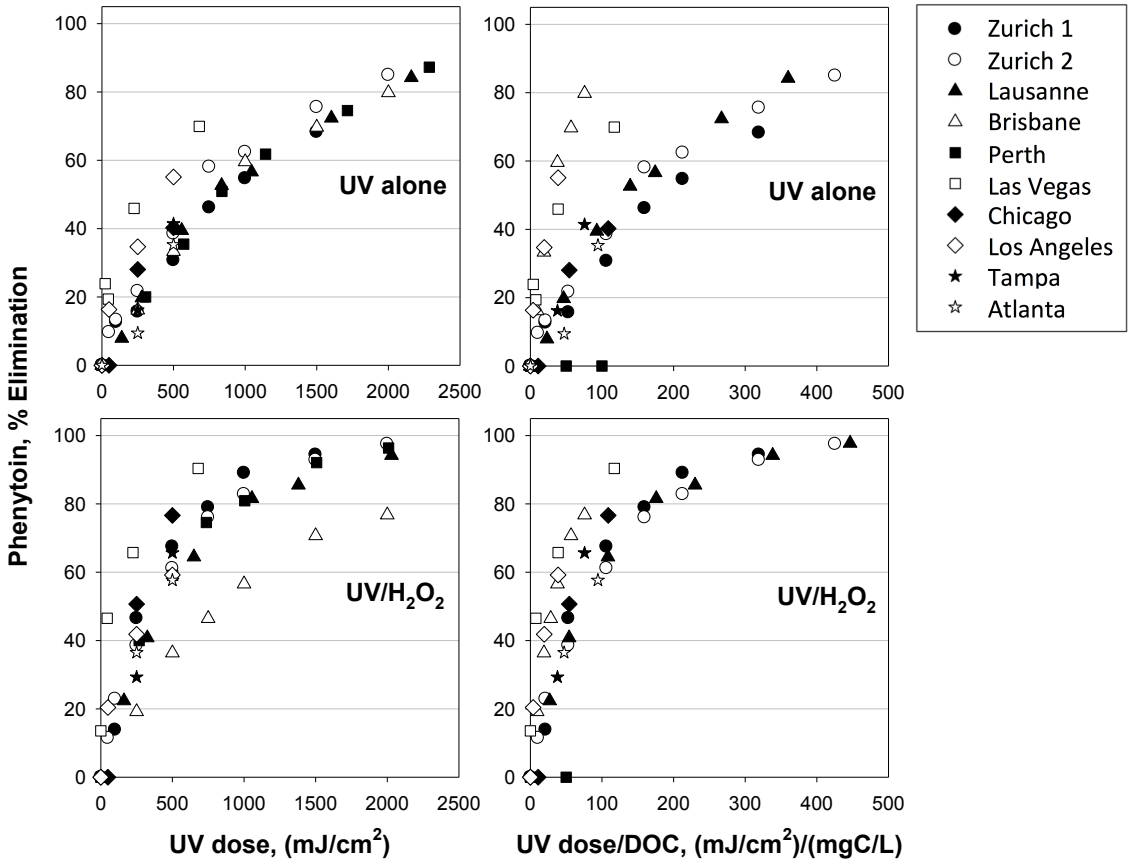

Figure S4E. Abatement of atrazine with UV and UV/H_2O_2 (10 mg/L of H_2O_2). Abatement levels are reported as a function of UV dose (left) and UV dose normalized to DOC.

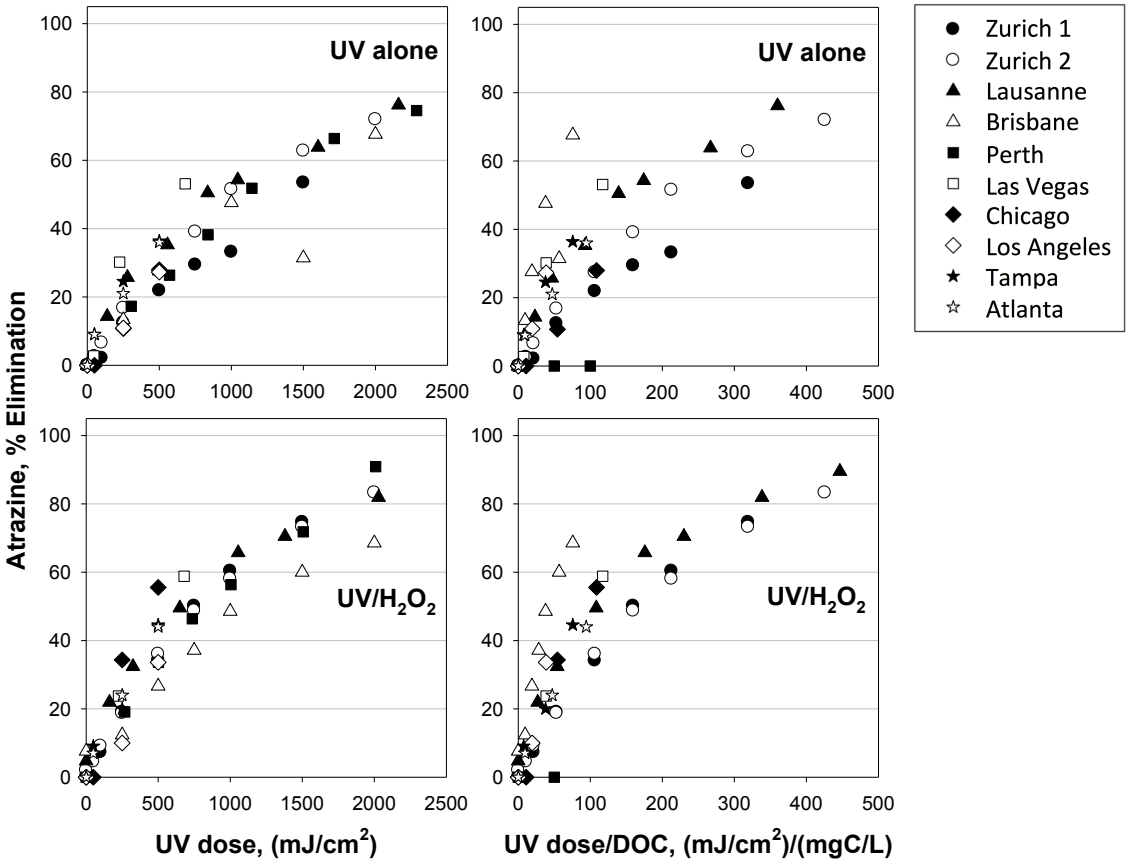

Figure S4F. Abatement of naproxen with UV and UV/H_2O_2 (10 mg/L of H_2O_2). Abatement levels are reported as a function of UV dose (left) and UV dose normalized to DOC.

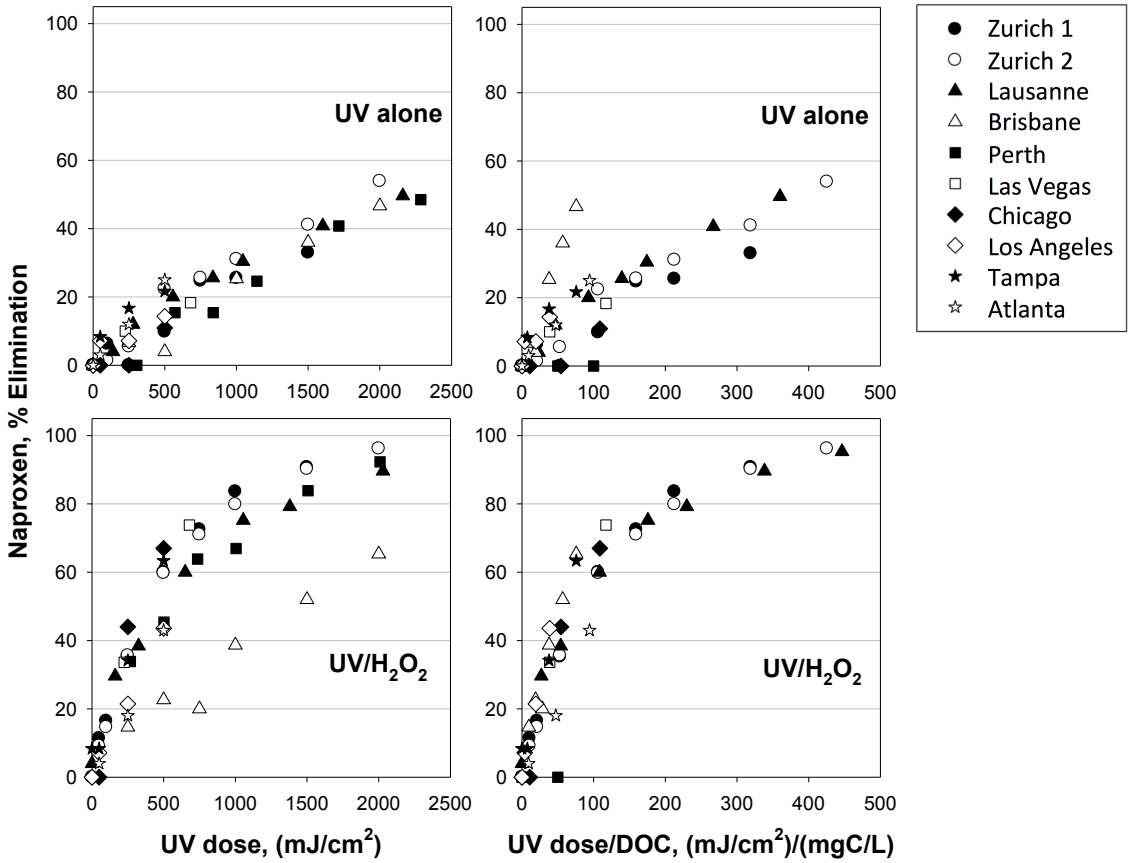

Figure S4G. Abatement of ibuprofen with UV and UV/H_2O_2 (10 mg/L of H_2O_2). Abatement levels are reported as a function of UV dose (left) and UV dose normalized to DOC.

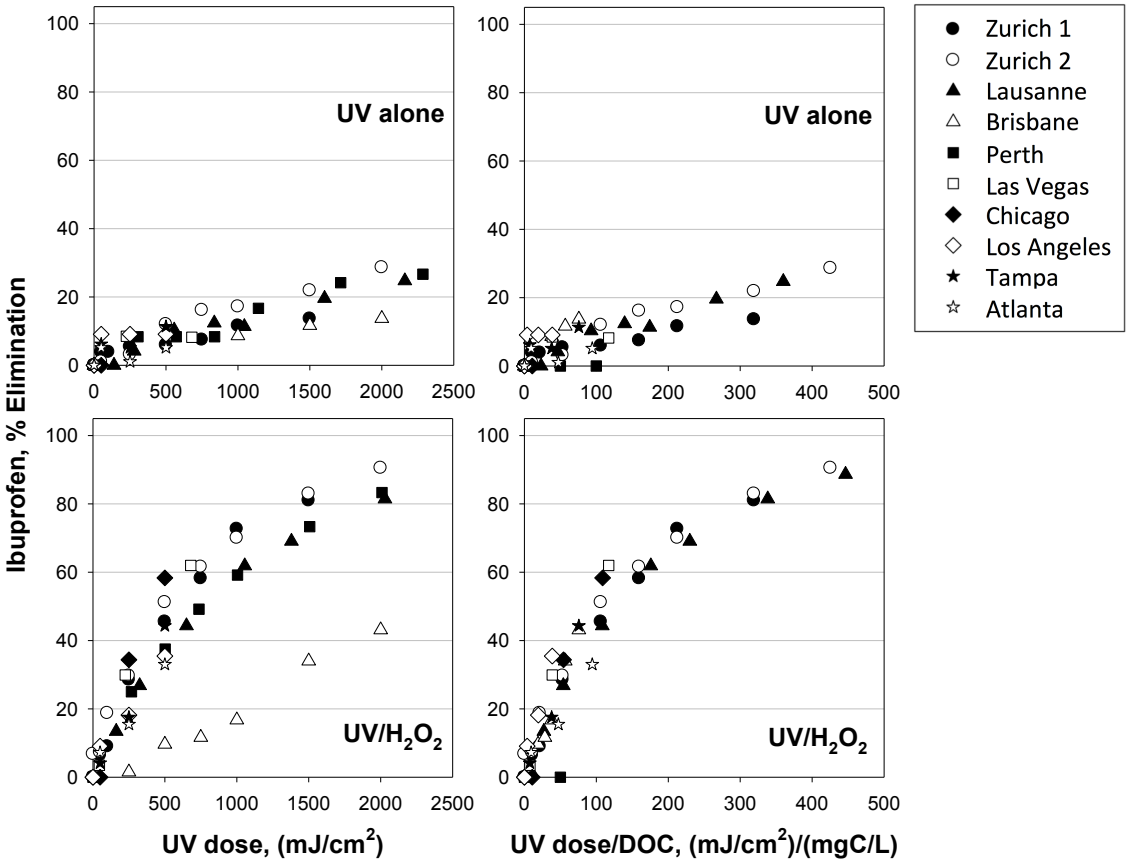

Figure S4H. Abatement of trimethoprim with UV and UV/H_2O_2 (10 mg/L of H_2O_2). Abatement levels are reported as a function of UV dose (left) and UV dose normalized to DOC.

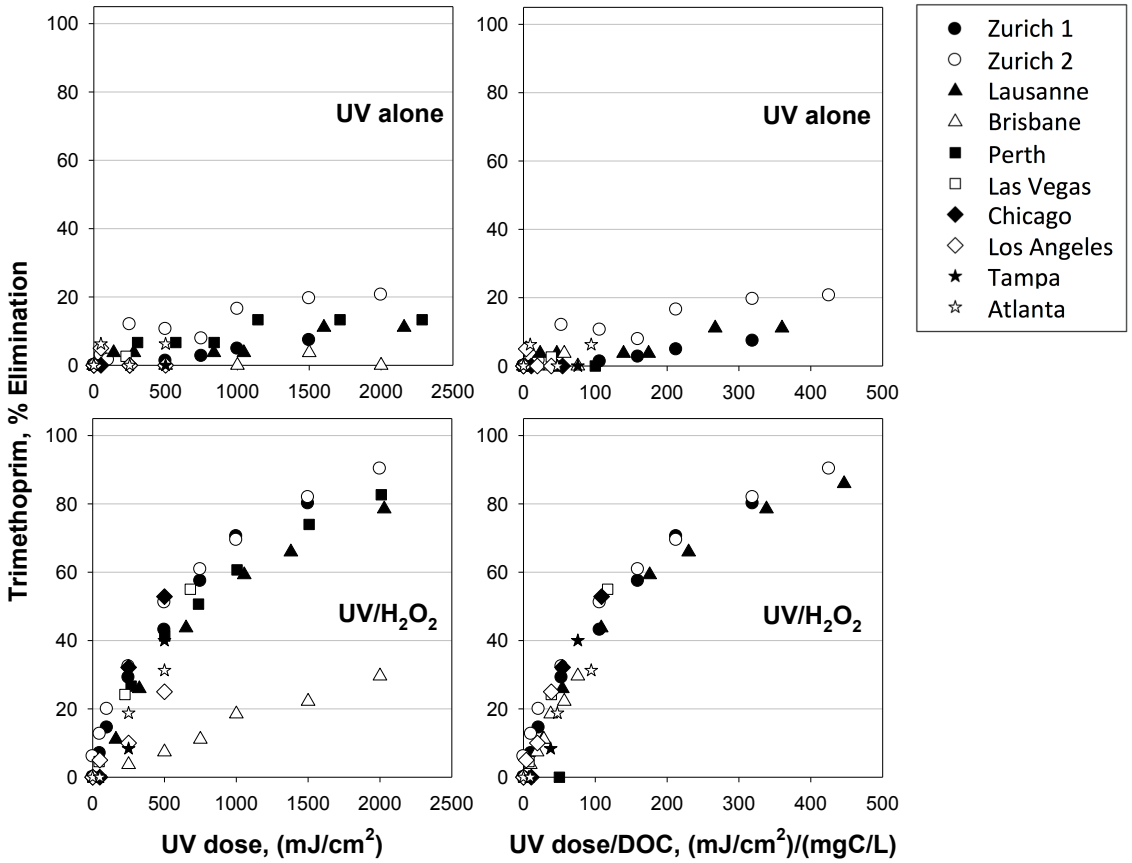

Figure S4I. Abatement of atenolol with UV and UV/H_2O_2 (10 mg/L of H_2O_2). Abatement levels are reported as a function of UV dose (left) and UV dose normalized to DOC.

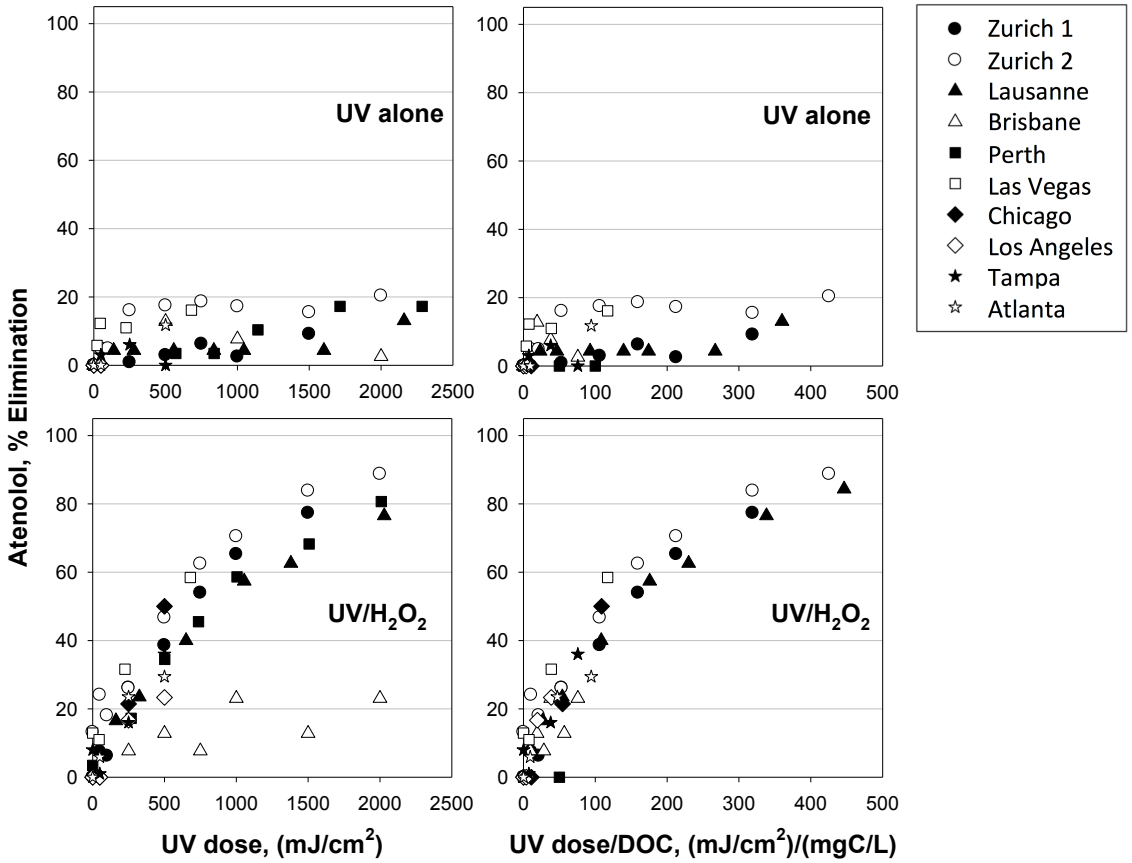

Figure S4J. Abatement of DEET with UV and UV/H_2O_2 (10 mg/L of H_2O_2). Abatement levels are reported as a function of UV dose (left) and UV dose normalized to DOC.

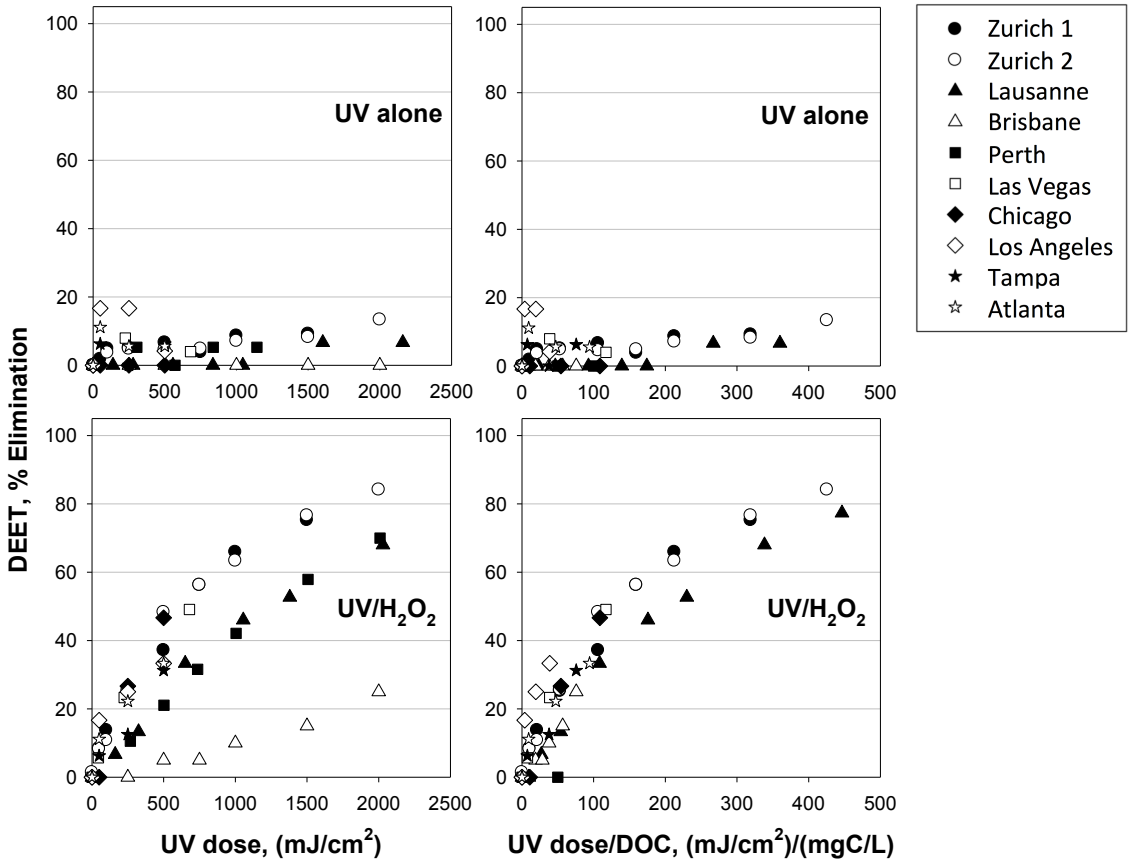

Figure S4K. Abatement of carbamazepine with UV and UV/H_2O_2 (10 mg/L of H_2O_2). Abatement levels are reported as a function of UV dose (left) and UV dose normalized to DOC.

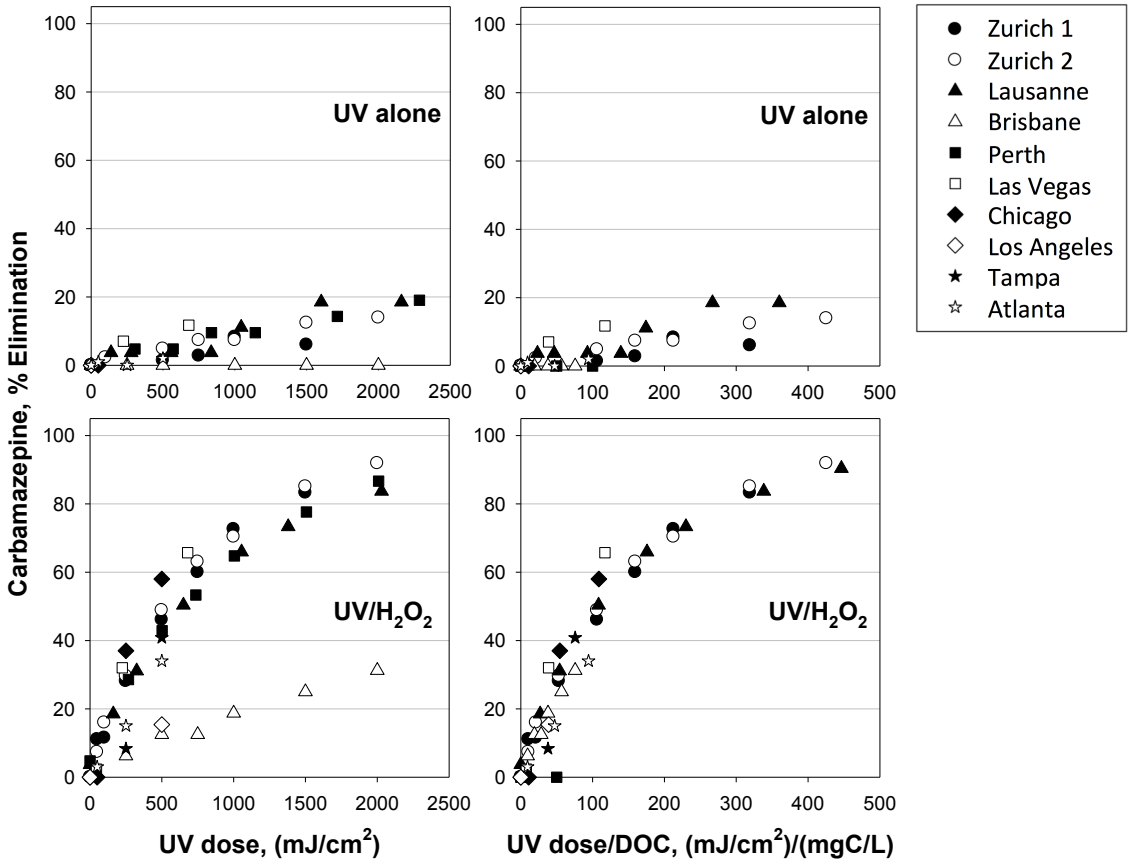

Figure S4L. Abatement of gemfibrozil with UV and UV/H_2O_2 (10 mg/L of H_2O_2). Abatement levels are reported as a function of UV dose (left) and UV dose normalized to DOC.

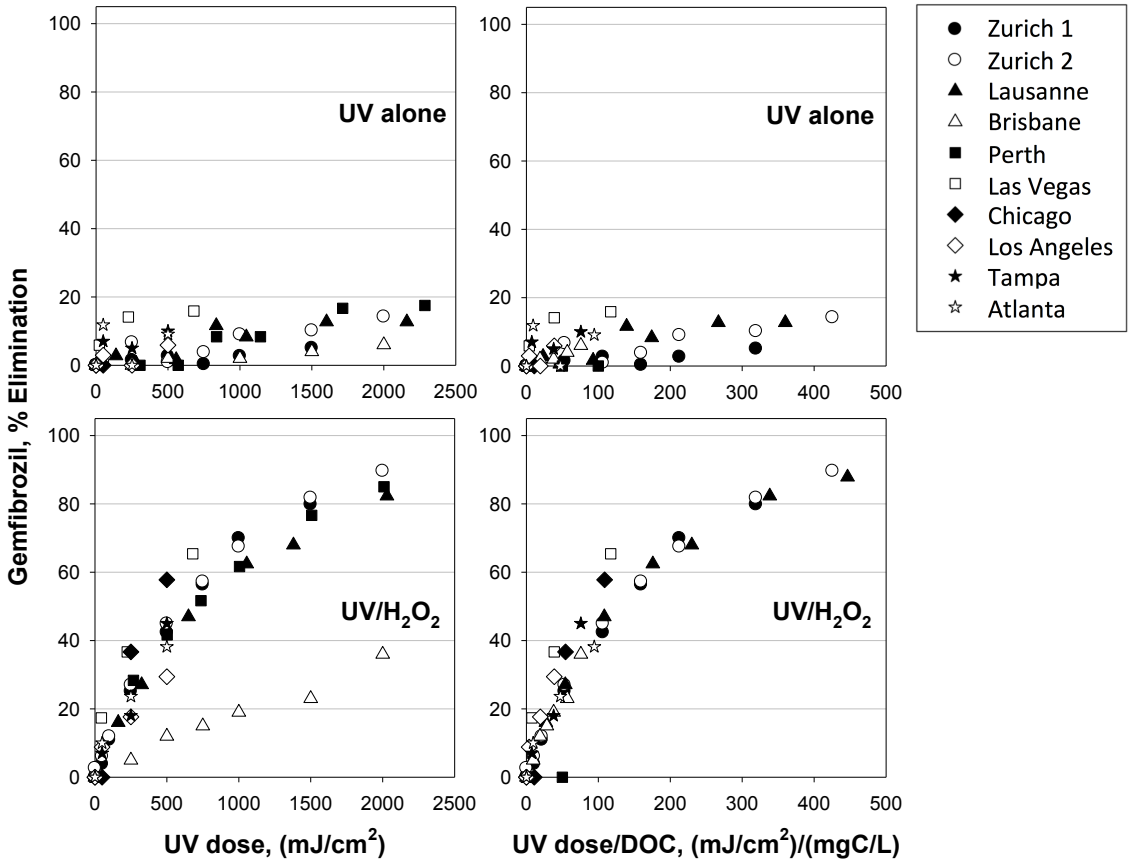

Figure S4M. Abatement of primidone with UV and UV/H_2O_2 (10 mg/L of H_2O_2). Abatement levels are reported as a function of UV dose (left) and UV dose normalized to DOC.

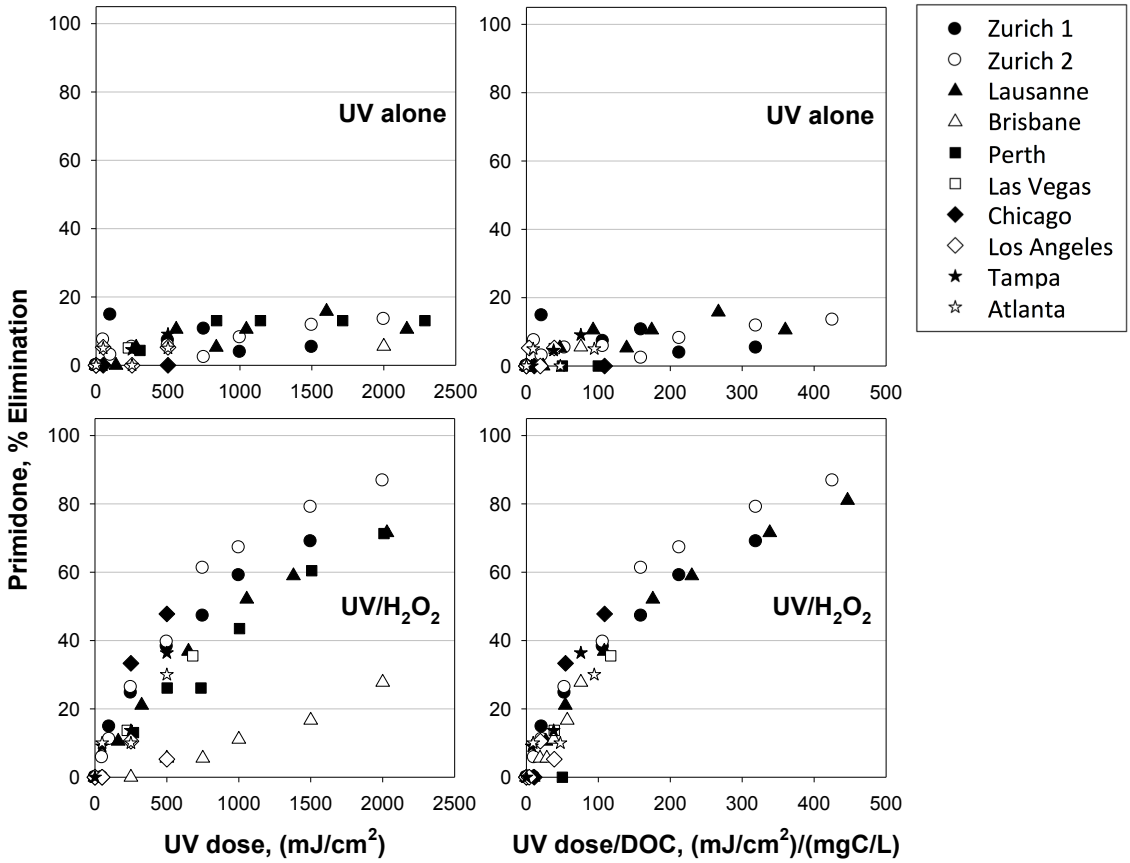

Figure S4N. Abatement of bisphenol A with UV and UV/H_2O_2 (10 mg/L of H_2O_2). Abatement levels are reported as a function of UV dose (left) and UV dose normalized to DOC.

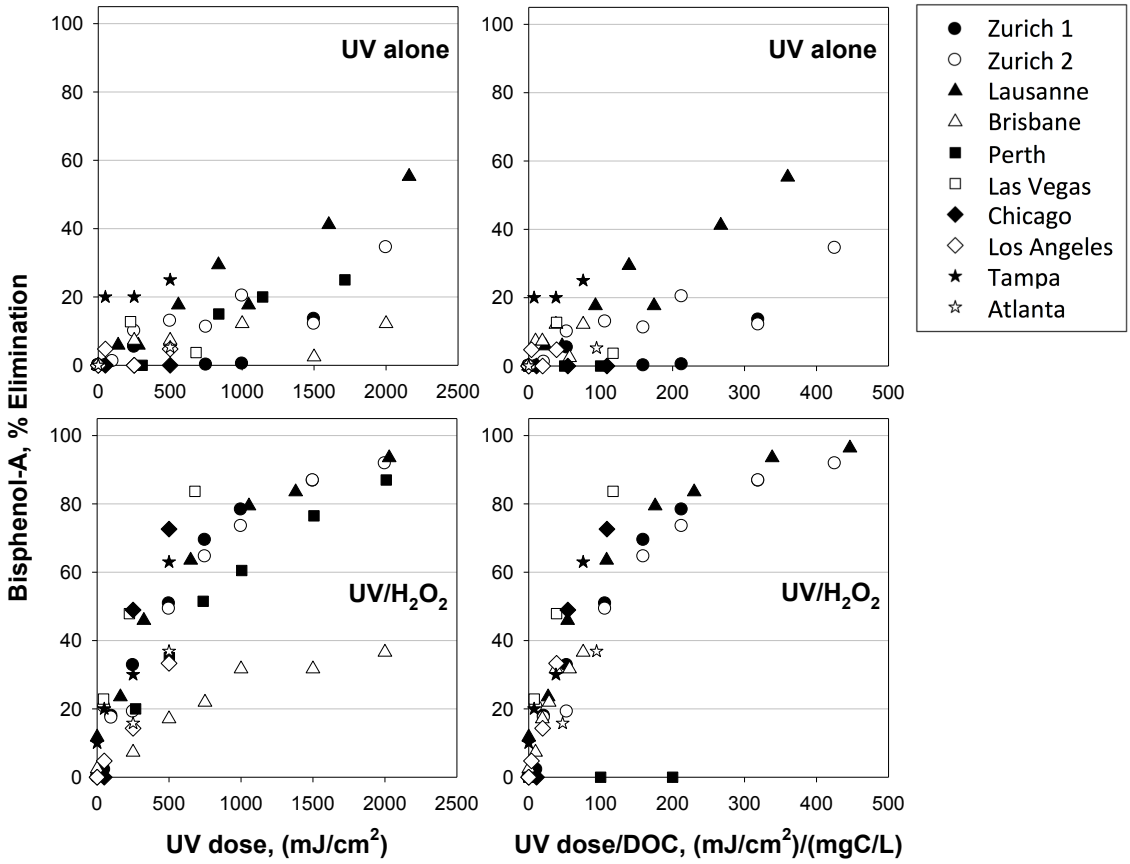

Figure S4O. Abatement of meprobamate with UV and UV/H_2O_2 (10 mg/L of H_2O_2). Abatement levels are reported as a function of UV dose (left) and UV dose normalized to DOC.

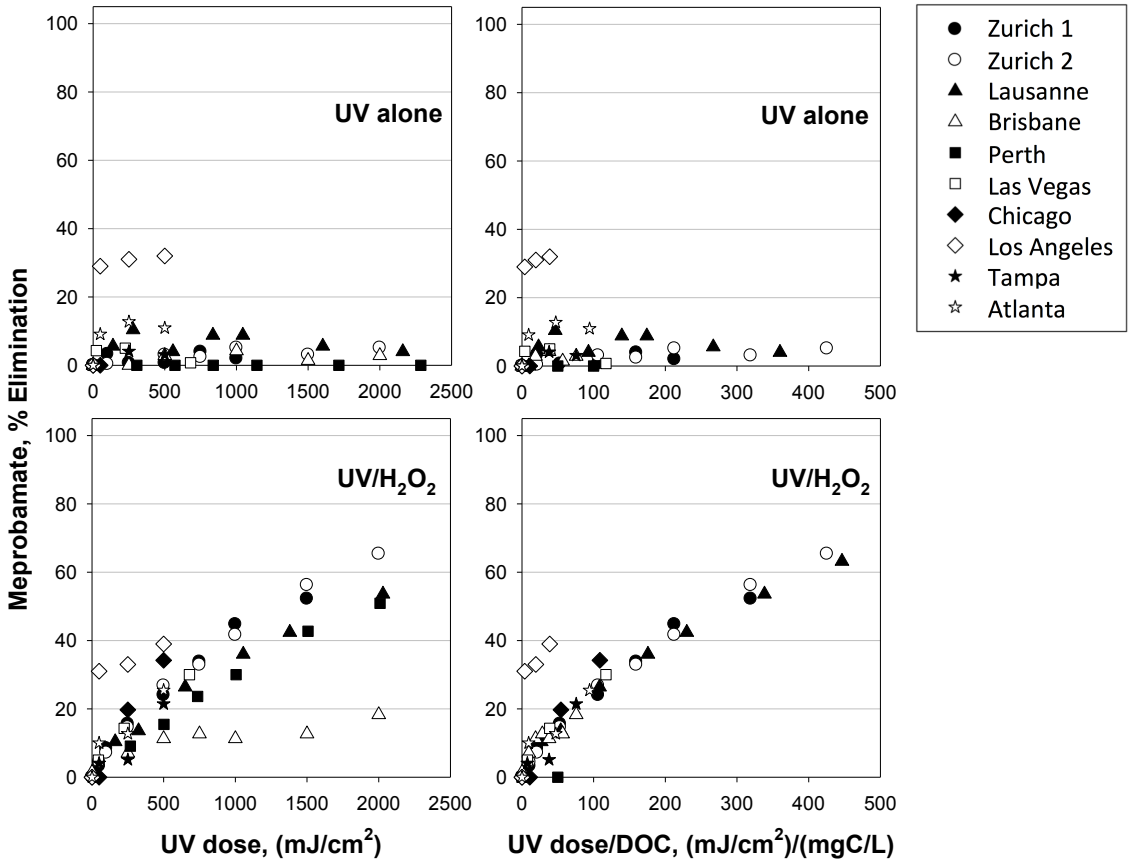

Figure S5. Determination of pseudo first order rate constants ($k_{UV/DOC}$) with respect to DOC-normalized UV dose for the photo-resistant compounds in this study ($k_{i,UV}<2\times10^{-4}$ $(mJ/cm^2)^{-1}$). The figures on the left are plotted against UV dose, while the figures on the right are plotted against the DOC-normalized UV dose to account for the effects of •OH scavenging by EfOM during the UV/H_2O_2 experiments (10 mg/L of H_2O_2).

Atenolol:

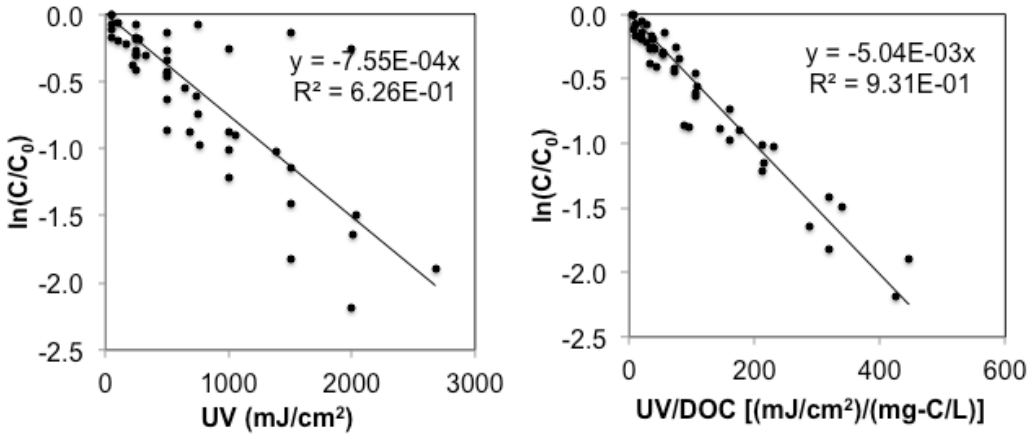

Bisphenol A:

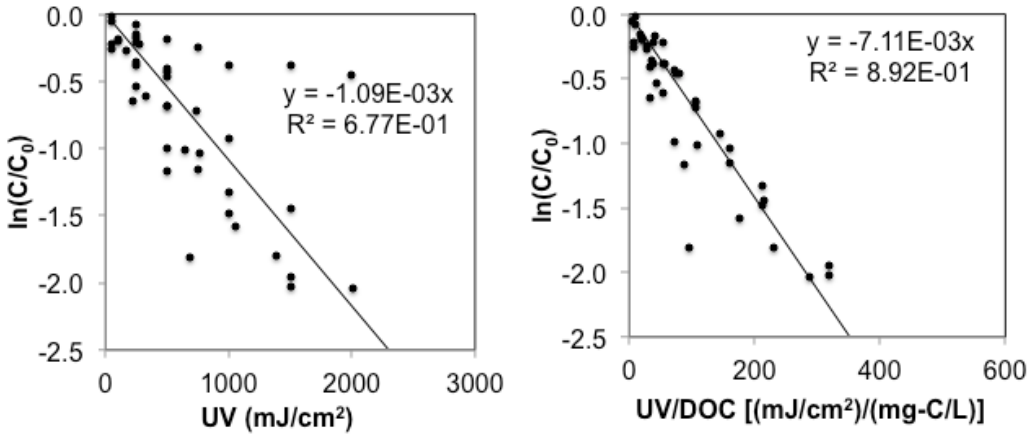

Carbamazepine:

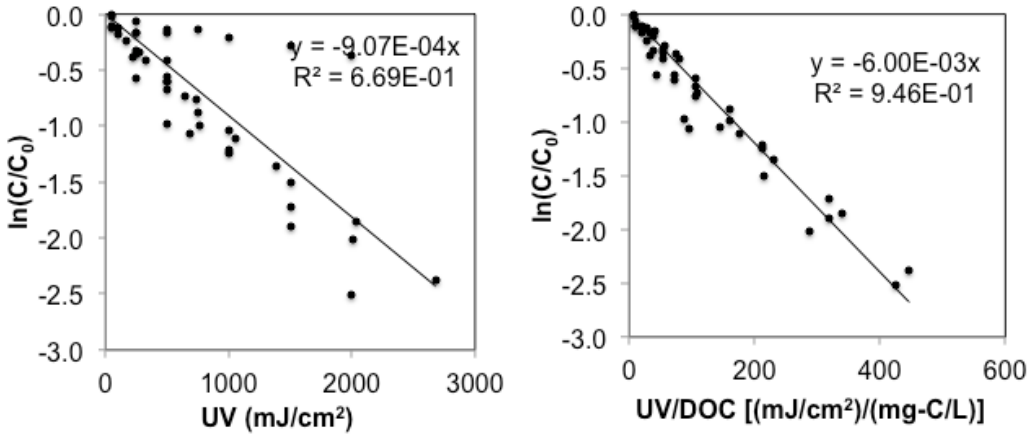

Figure S5 (cont.). Determination of pseudo first order rate constants ($k_{UV/DOC}$) with respect to DOC-normalized UV dose for the photo-resistant compounds in this study ($k_{i,UV}<2\times10^{-4}$ $(mJ/cm^2)^{-1}$). The figures on the left are plotted against UV dose, while the figures on the right are plotted against the DOC-normalized UV dose to account for the effects of •OH scavenging by EfOM during the UV/H_2O_2 experiments (10 mg/L of H_2O_2).

DEET:

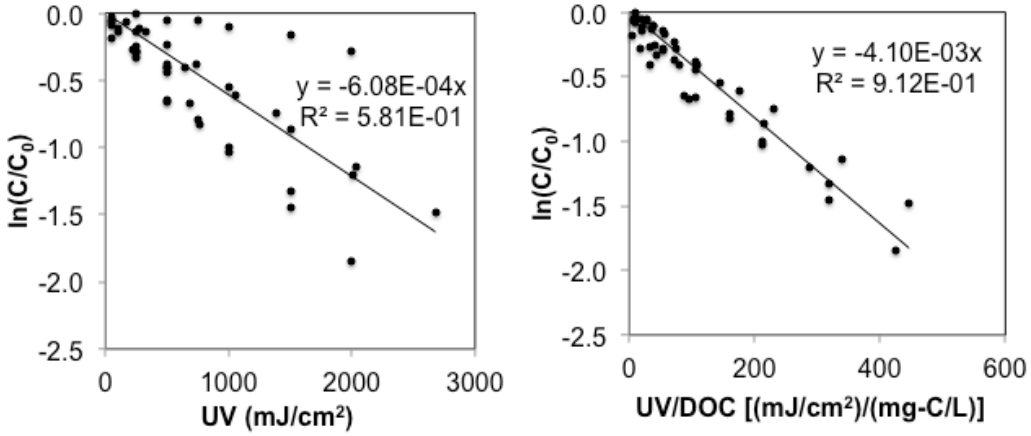

Gemfibrozil:

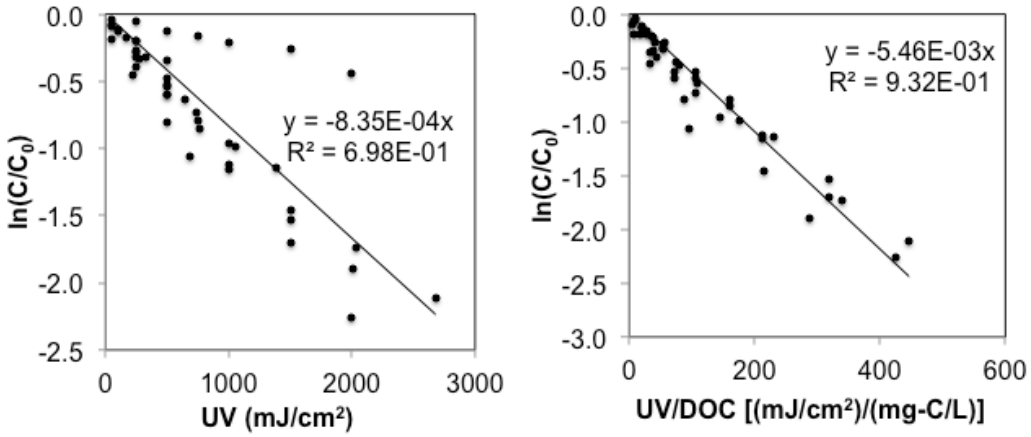

Ibuprofen:

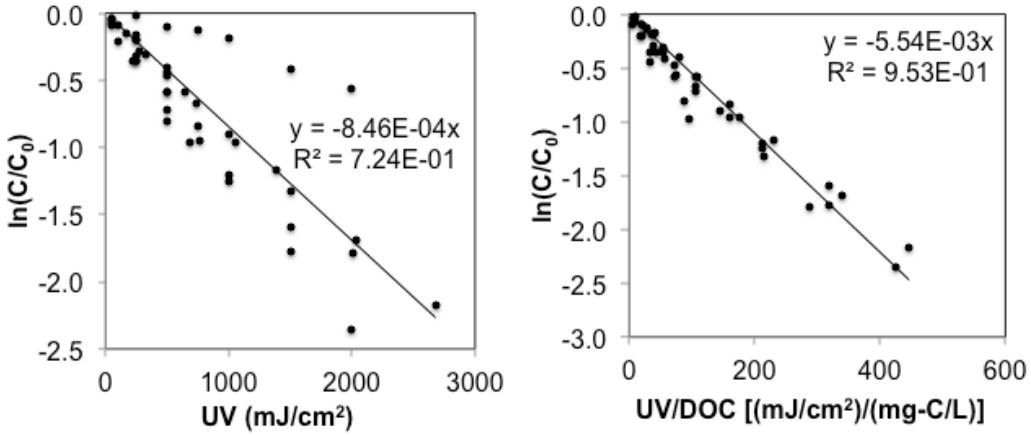

Figure S5 (cont.). Determination of pseudo first order rate constants ($k_{UV/DOC}$) with respect to DOC-normalized UV dose for the photo-resistant compounds in this study ($k_{i,UV}<2\times10^{-4}$ $(mJ/cm^2)^{-1}$). The figures on the left are plotted against UV dose, while the figures on the right are plotted against the DOC-normalized UV dose to account for the effects of •OH scavenging by EfOM during the UV/H_2O_2 experiments (10 mg/L of H_2O_2).

Meprobamate:

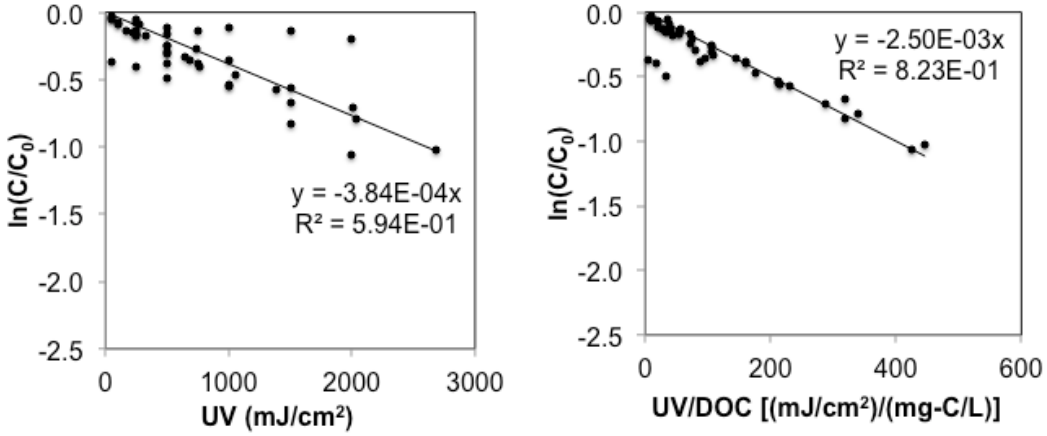

Primidone:

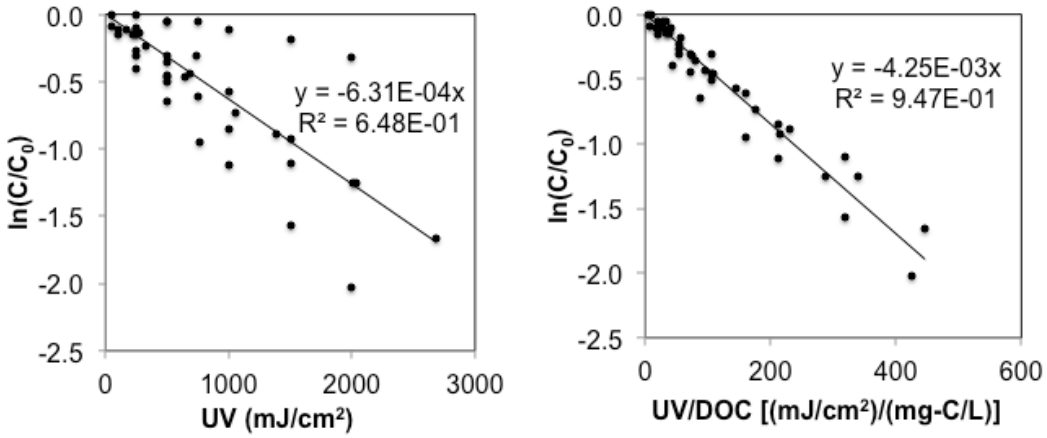

Trimethoprim:

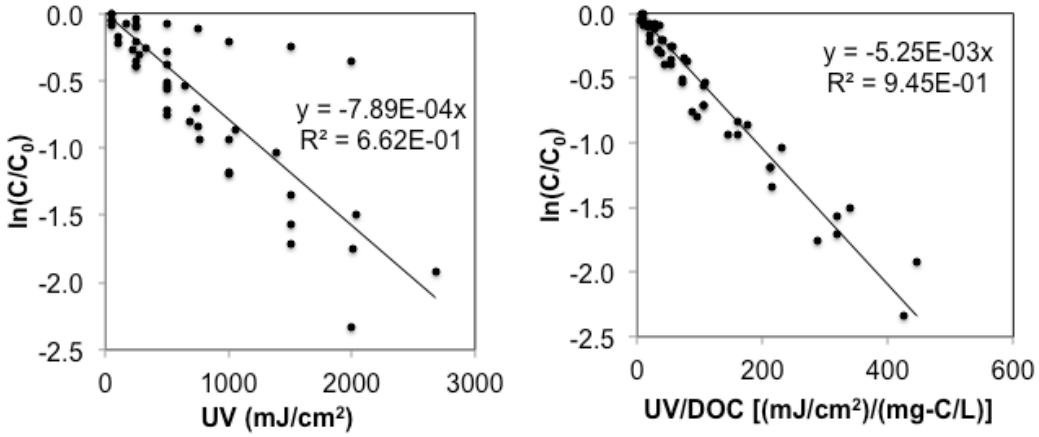

Text S2. Selection of surrogate parameters for bulk organic matter correlations.

UV alone achieved minimal transformation of bulk organic matter even at high UV doses, while UV/H_2O_2 resulted in more discernable decreases in absorbance at many wavelengths. Absorbance spectra are provided for the U.S. wastewaters in Figures S5A-S9A. The maximum differentials occurred at wavelengths between 250 and 270 nm, and the relative differentials (i.e., $1\text{-}A/A_0$) offered easily decipherable peaks or plateaus between 250 and 300 nm (Figures S5B-S9B). Similar results, albeit to a greater extent, were observed for ozone and ozone/H_2O_2 in Gerrity et al. (2012).

With respect to fluorescence, EEM regions associated with proteins and microbial biopolymers (region I) and fulvic-like substances (region II) experienced consistent reductions in fluorescence, while humic-like substances (region III) exhibited slight increases at low UV doses (<100 mJ/cm^2) and overall decreases at higher UV doses (>100 mJ/cm^2) (data not shown). Example fluorescence spectra (λ_{ex}=254 nm) illustrating changes in regions I (λ_{em}=300-380 nm) and II (λ_{em}=380-480 nm) are illustrated in Figures S5C-S9C, and the corresponding relative differential fluorescence spectra (i.e., $1\text{-}F/F_0$) are illustrated in Figures S5D-S9D. Interestingly, the U.S. wastewaters with the highest scavenging contribution from EfOM (Los Angeles and Atlanta; Figure 3) were also characterized by prominent protein or region I peaks relative to their fulvic-like or region 2 peaks (Figures S7C and S9C). Consistent with Gerrity et al. (2012), differential UV_{254} absorbance and total fluorescence (i.e., integrated EEM for all regions; Figure S10) were selected for the development of the correlation models.

Figure S6. Examples of changes in bulk organic matter as a function of UV dose (with 10 mg/L H_2O_2) in Las Vegas secondary effluent samples: (A) absorbance spectra, (B) relative differential absorbance spectra, (C) fluorescence spectra (arbitrary fluorescence units) at an excitation wavelength of 254 nm, and (D) relative differential fluorescence spectra at an excitation wavelength of 254 nm.

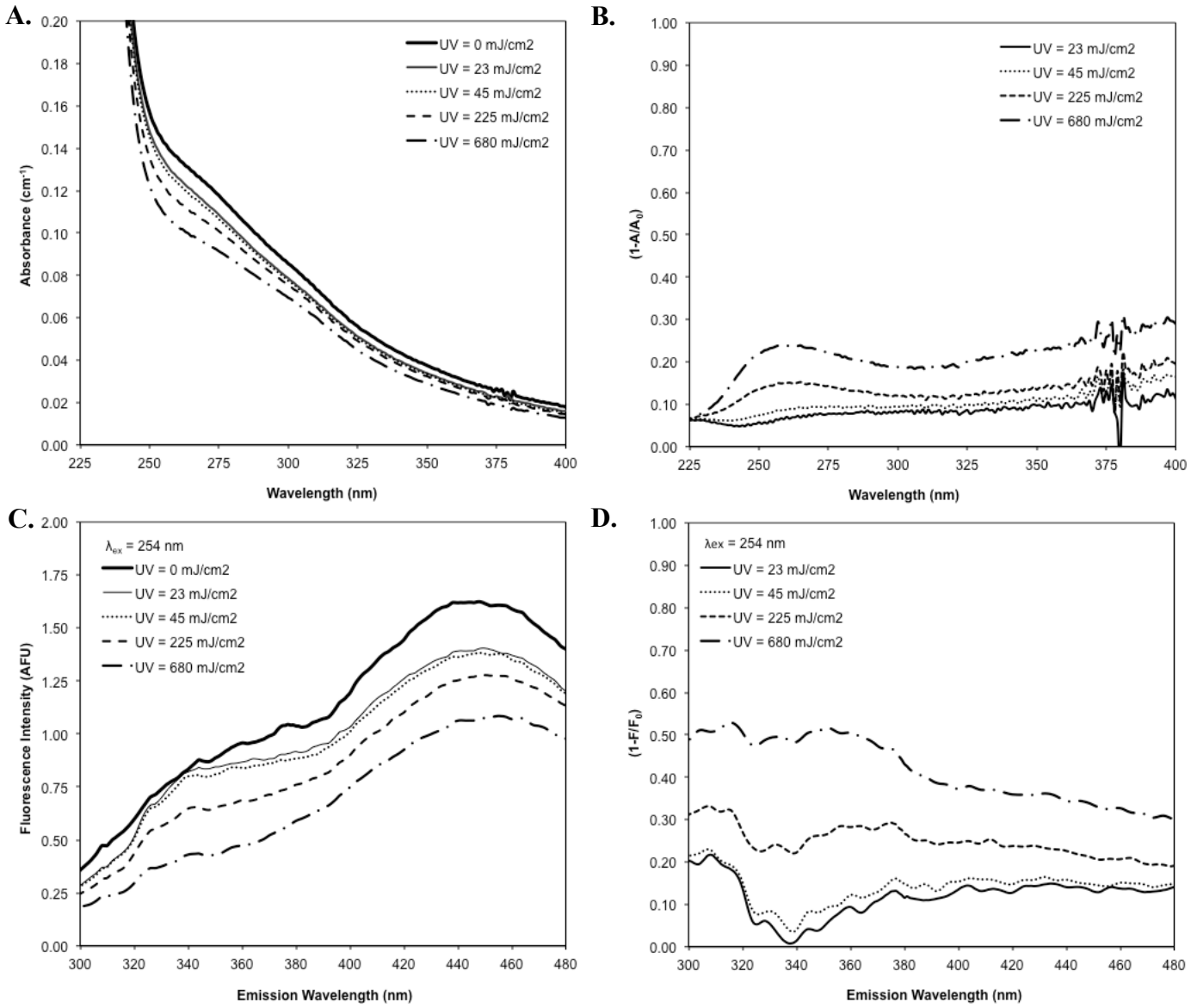

Figure S7. Examples of changes in bulk organic matter as a function of UV dose (with 10 mg/L H_2O_2) in Chicago secondary effluent samples: (A) absorbance spectra, (B) relative differential absorbance spectra, (C) fluorescence spectra (arbitrary fluorescence units) at an excitation wavelength of 254 nm, and (D) relative differential fluorescence spectra at an excitation wavelength of 254 nm.

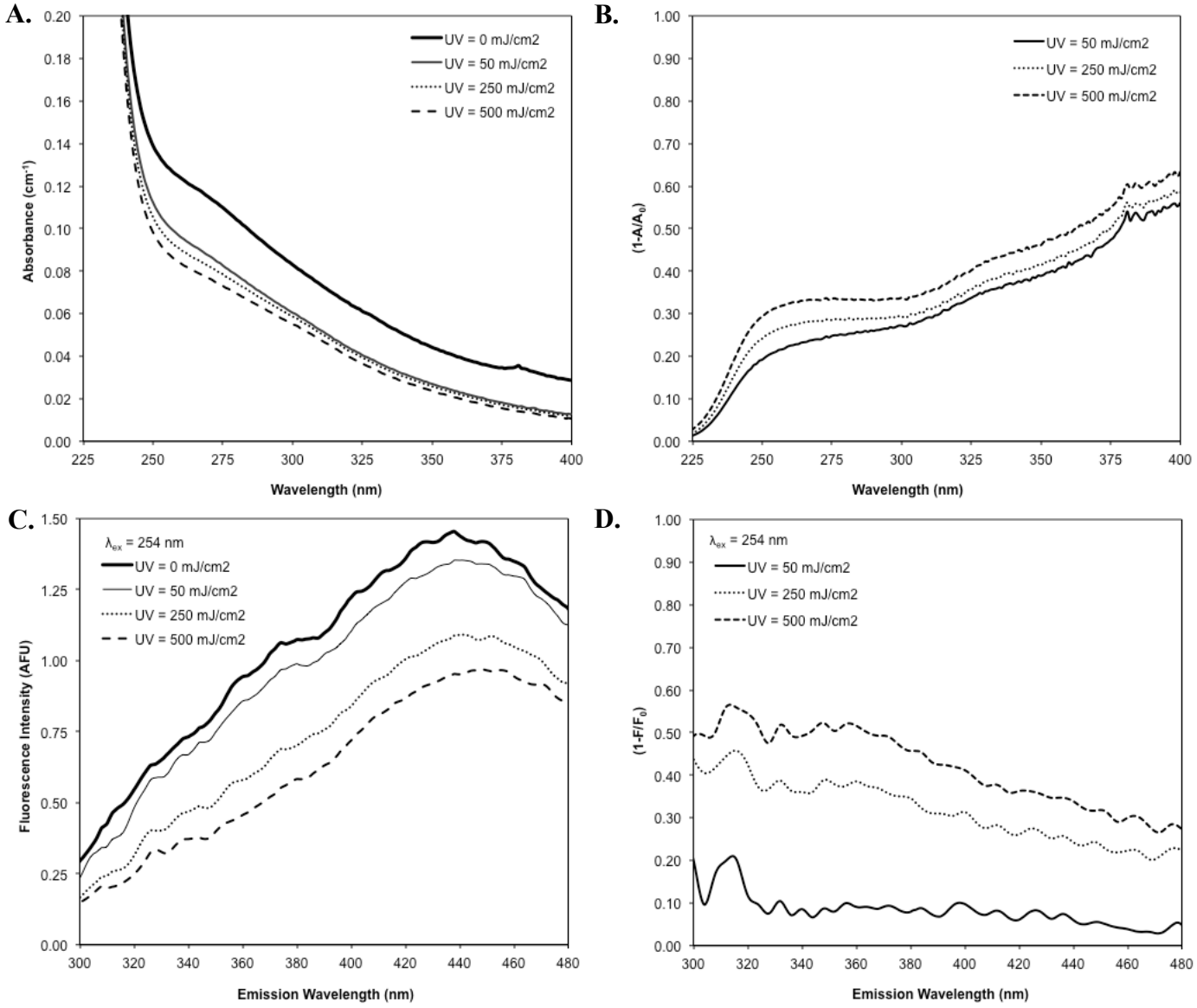

Figure S8. Examples of changes in bulk organic matter as a function of UV dose (with 10 mg/L H_2O_2) in Los Angeles secondary effluent samples: (A) absorbance spectra, (B) relative differential absorbance spectra, (C) fluorescence spectra (arbitrary fluorescence units) at an excitation wavelength of 254 nm, and (D) relative differential fluorescence spectra at an excitation wavelength of 254 nm.

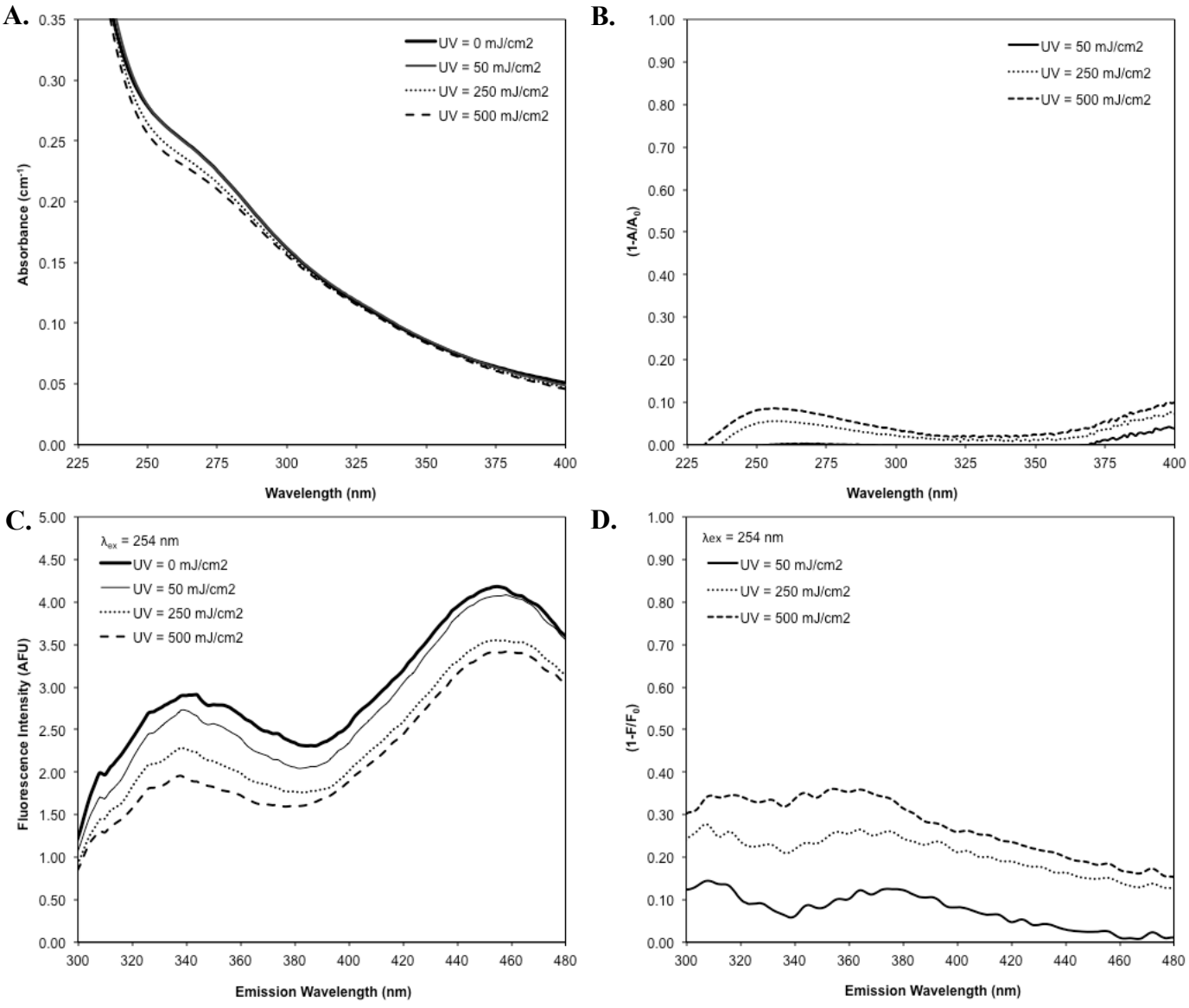

Figure S9. Examples of changes in bulk organic matter as a function of UV dose (with 10 mg/L H_2O_2) in Tampa secondary effluent samples: (A) absorbance spectra, (B) relative differential absorbance spectra, (C) fluorescence spectra (arbitrary fluorescence units) at an excitation wavelength of 254 nm, and (D) relative differential fluorescence spectra at an excitation wavelength of 254 nm.

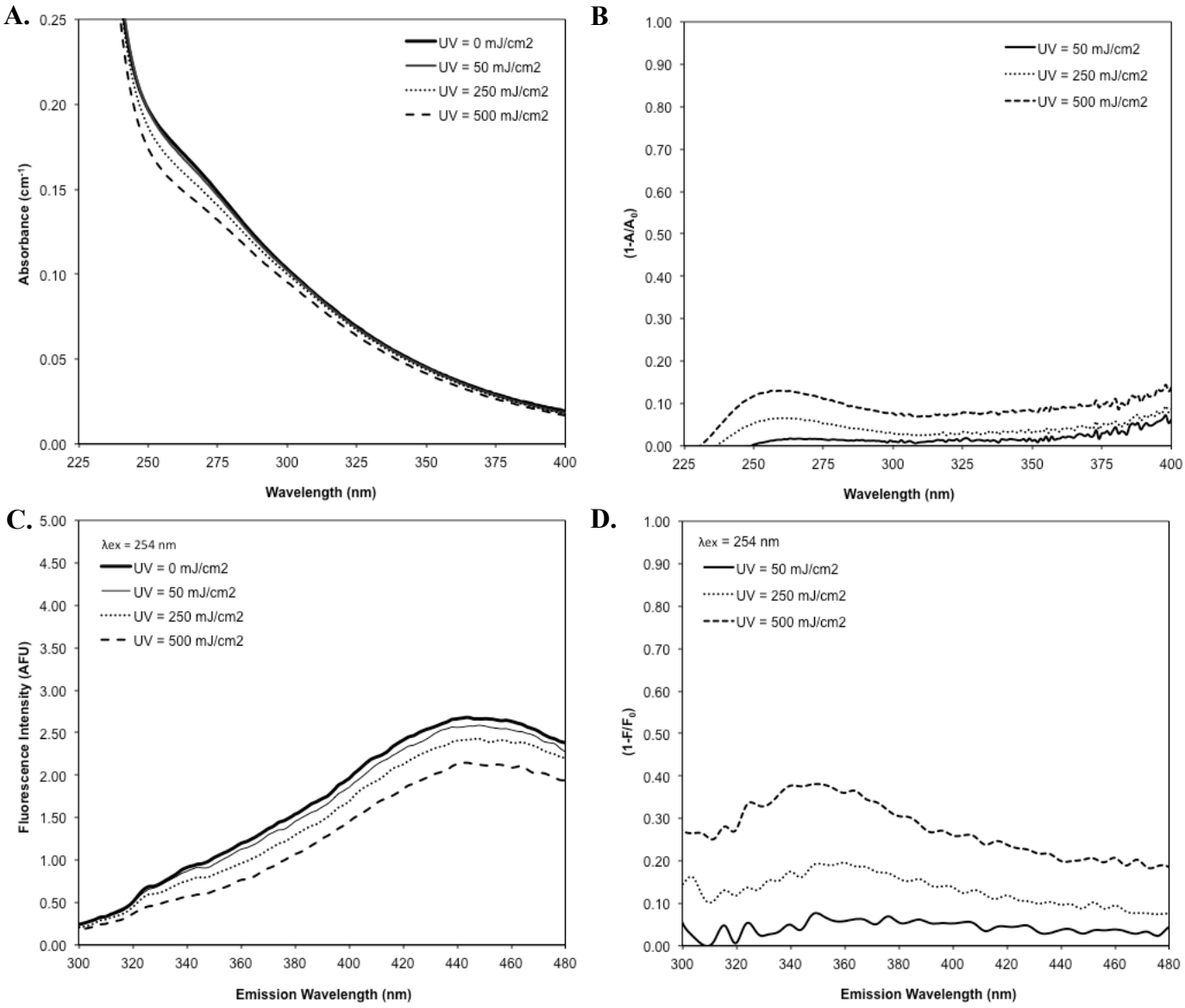

Figure S10. Examples of changes in bulk organic matter as a function of UV dose (with 10 mg/L H_2O_2) in Atlanta secondary effluent samples: (A) absorbance spectra, (B) relative differential absorbance spectra, (C) fluorescence spectra (arbitrary fluorescence units) at an excitation wavelength of 254 nm, and (D) relative differential fluorescence spectra at an excitation wavelength of 254 nm.

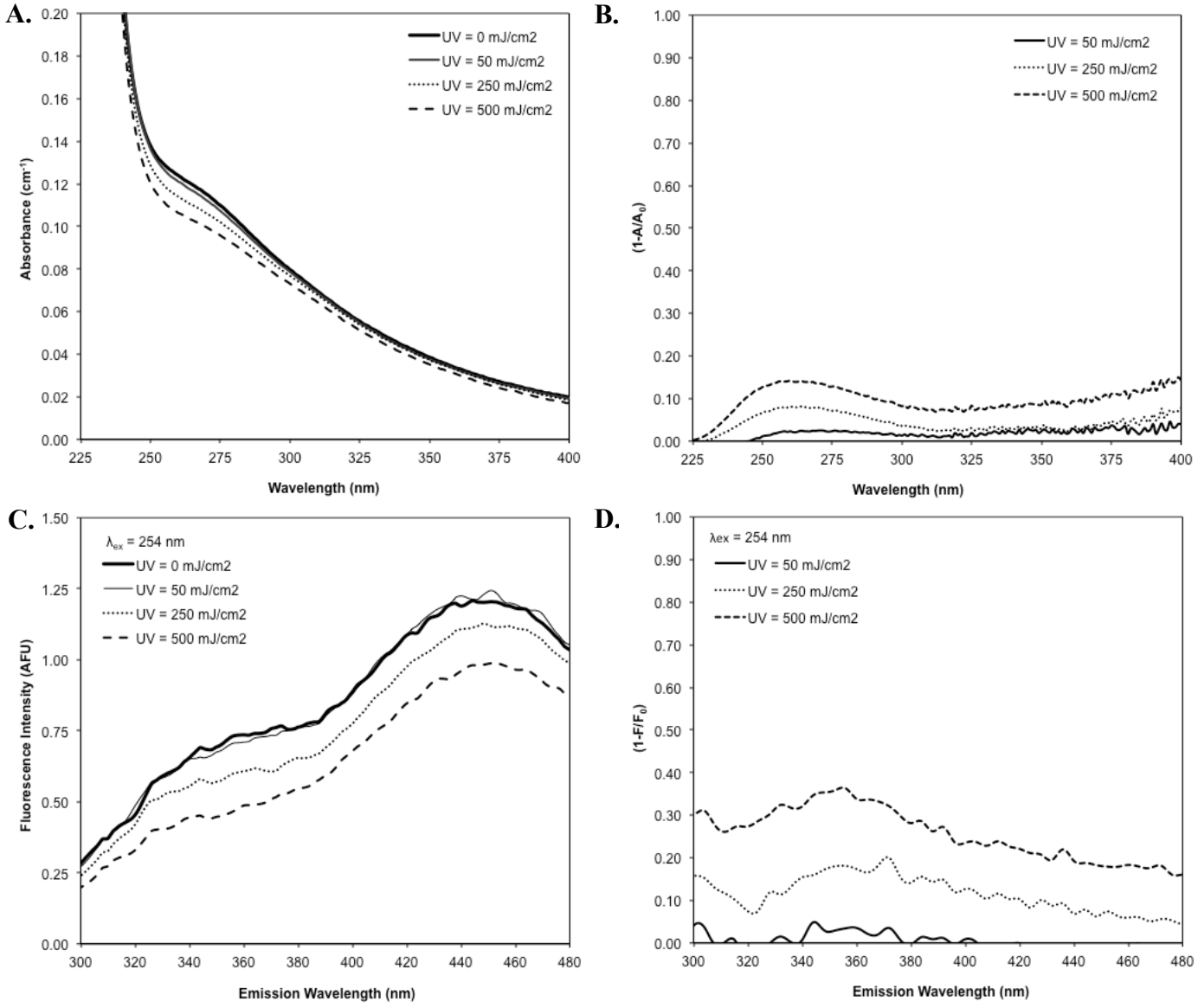

Figure S11. Summary of the excitation emission matrices (EEMs) for the UV/H_2O_2 process (10 mg/L H_2O_2). All EEMs have a fluorescence intensity scale from 0-1 arbitrary fluorescence units (AFU) to allow for direct comparisons between matrices.

Las Vegas:

UV = 0 mJ/cm² UV = 45 mJ/cm² UV = 225 mJ/cm² UV = 680 mJ/cm²

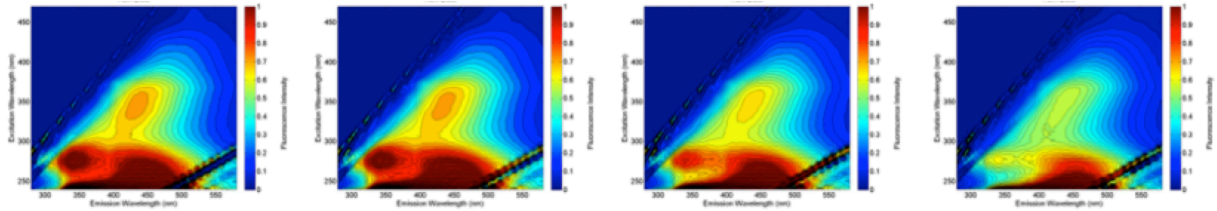

ΔTF=0% ΔTF=9% ΔTF=19% ΔTF=35%

Chicago:

UV = 0 mJ/cm² UV = 50 mJ/cm² UV = 250 mJ/cm² UV = 500 mJ/cm²

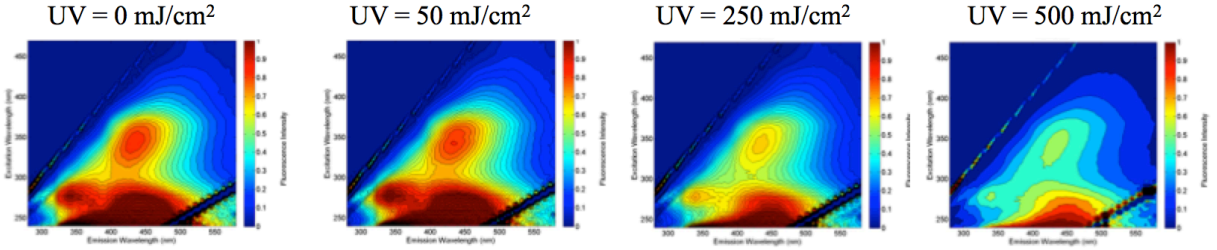

ΔTF=0% ΔTF=9% ΔTF=28% ΔTF=40%

Los Angeles:

UV = 0 mJ/cm² UV = 50 mJ/cm² UV = 250 mJ/cm² UV = 500 mJ/cm²

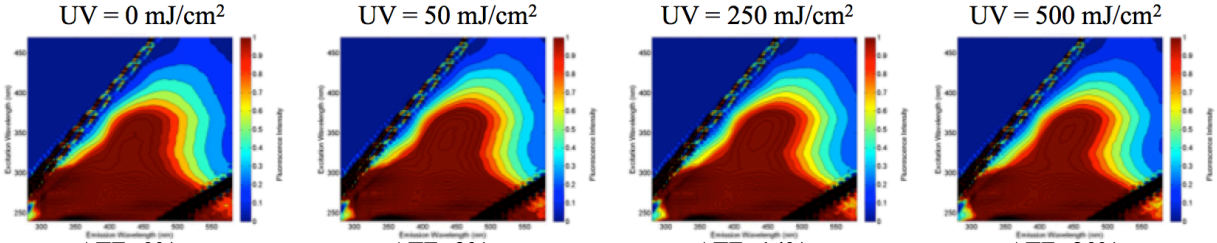

ΔTF=0% ΔTF=3% ΔTF=14% ΔTF=20%

Tampa:

UV = 0 mJ/cm² UV = 50 mJ/cm² UV = 250 mJ/cm² UV = 500 mJ/cm²

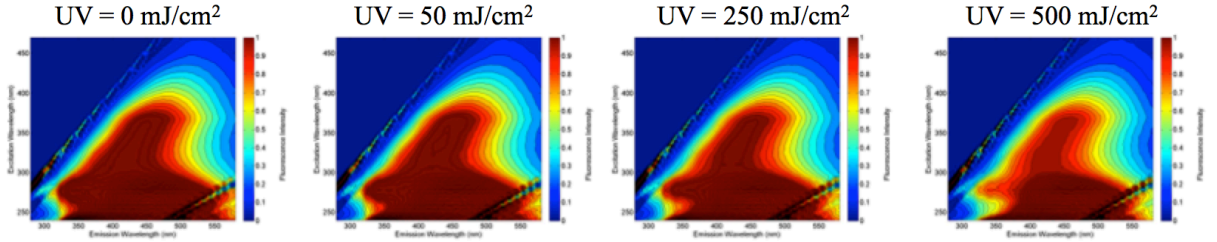

ΔTF=0% ΔTF=4% ΔTF=11% ΔTF=23%

Atlanta:

UV = 0 mJ/cm² UV = 50 mJ/cm² UV = 250 mJ/cm² UV = 500 mJ/cm²

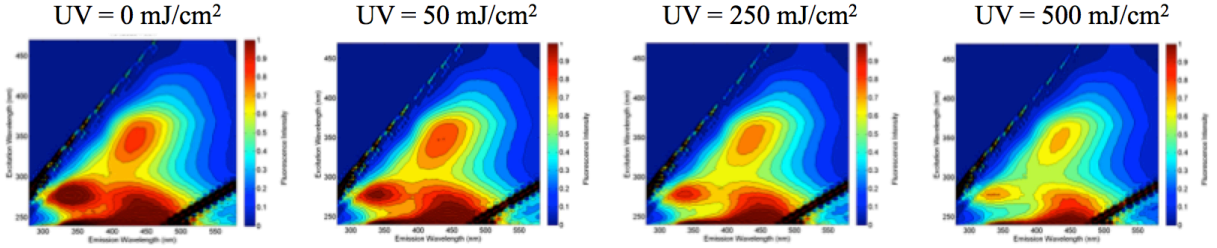

ΔTF=0% ΔTF=0% ΔTF=10% ΔTF=22%

Figure S12. Correlations between target compound oxidation and changes in bulk organic matter differentiated by secondary effluent (left and right) and by study (middle).

A.

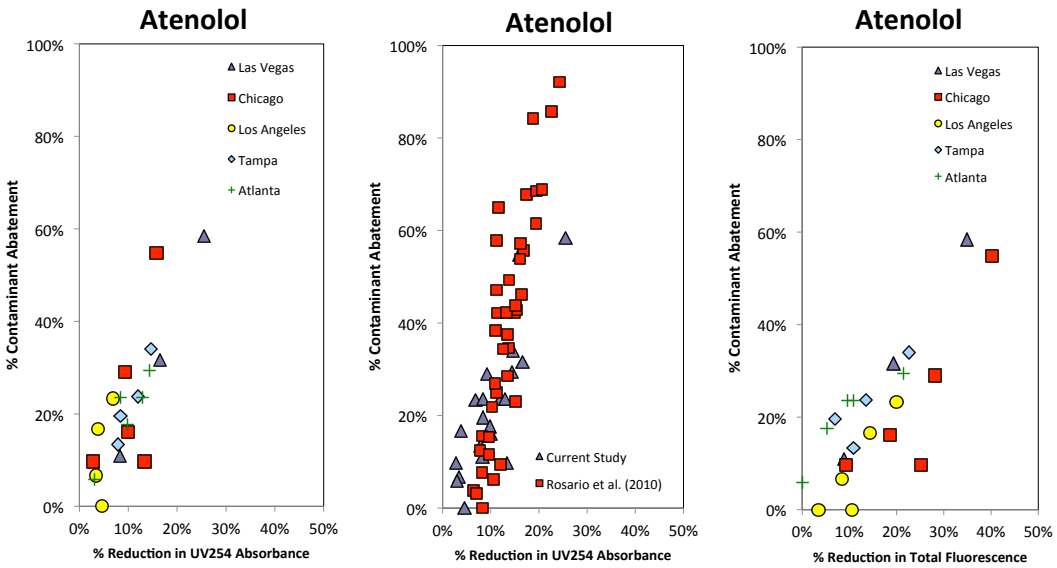

B.

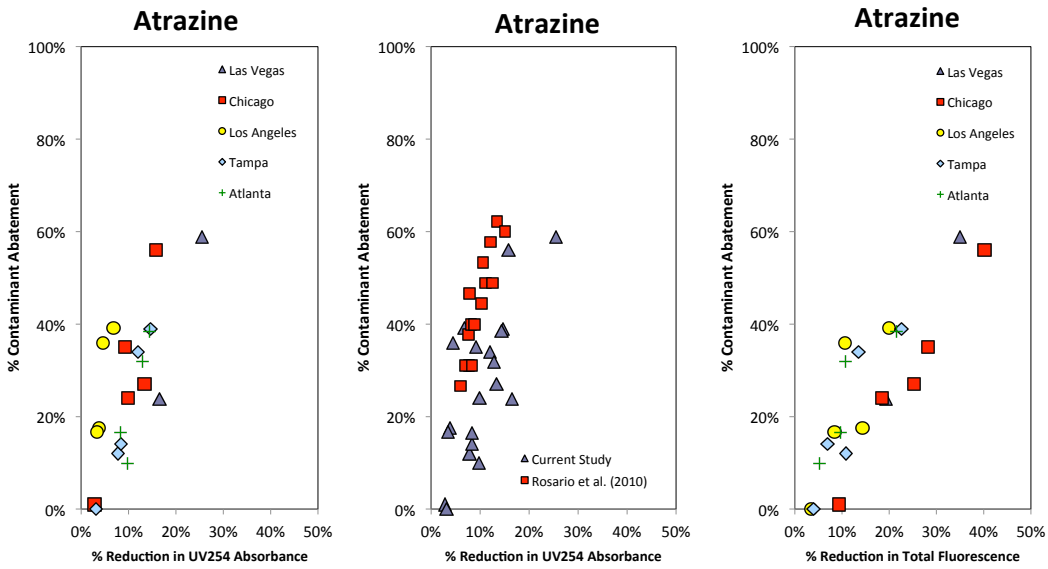

Figure S12. Correlations between target compound oxidation and changes in bulk organic matter differentiated by secondary effluent (left and right) and by study (middle).

C.

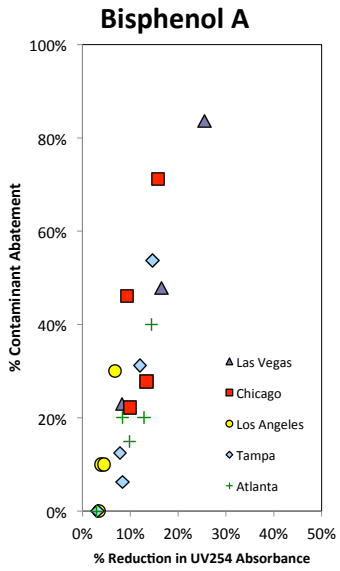

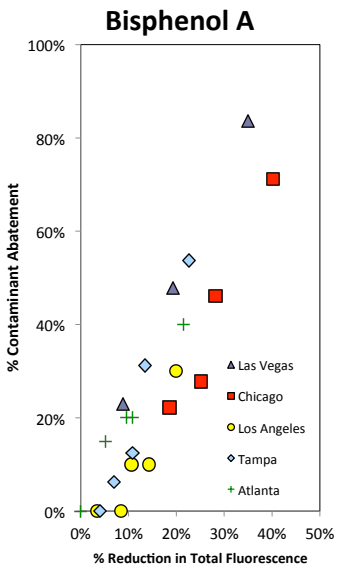

D.

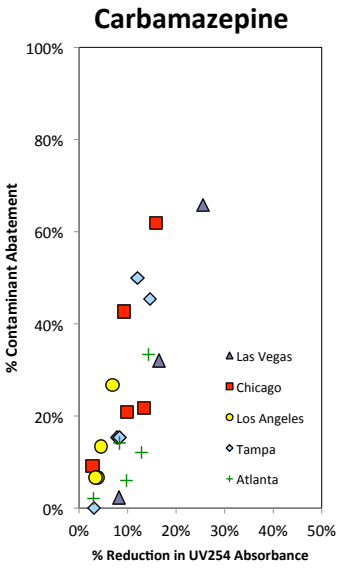

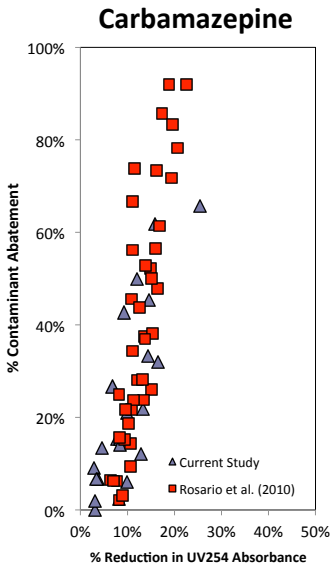

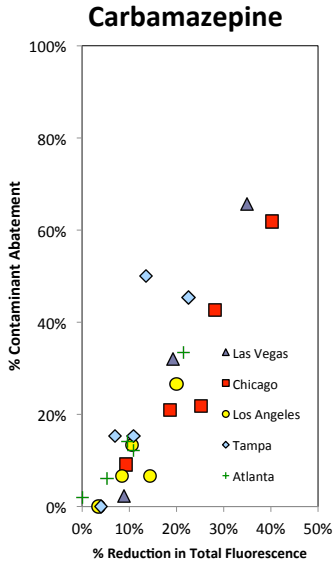

Figure S12. Correlations between target compound oxidation and changes in bulk organic matter differentiated by secondary effluent (left and right) and by study (middle).

E.

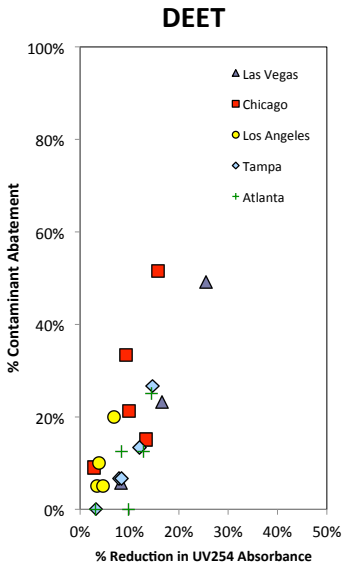

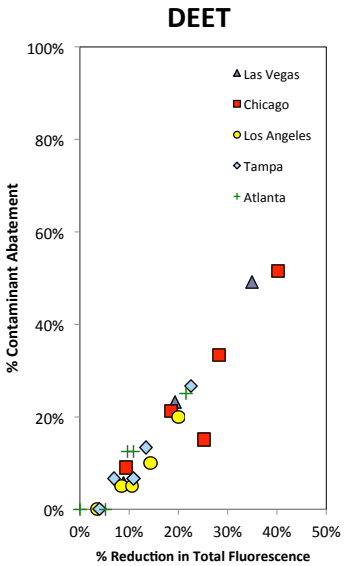

F.

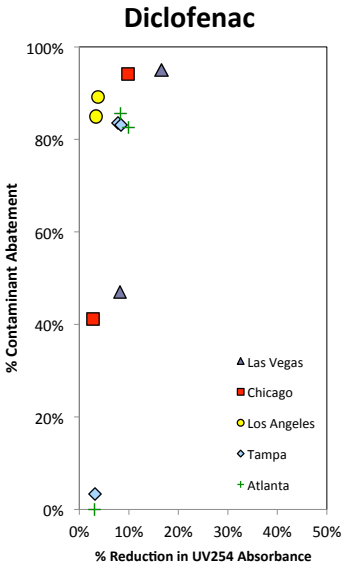

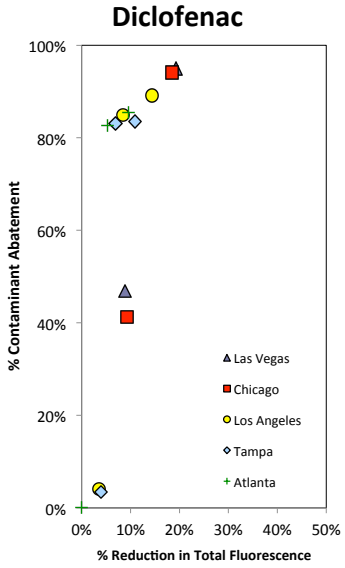

Figure S12. Correlations between target compound oxidation and changes in bulk organic matter differentiated by secondary effluent (left and right) and by study (middle).

G.

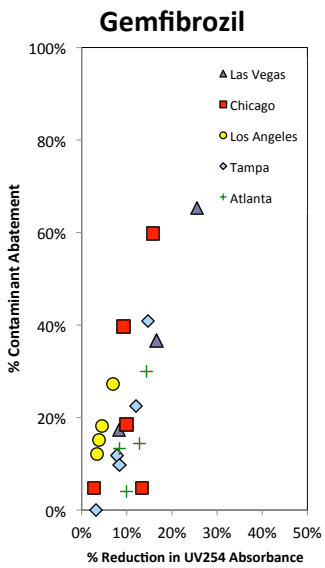

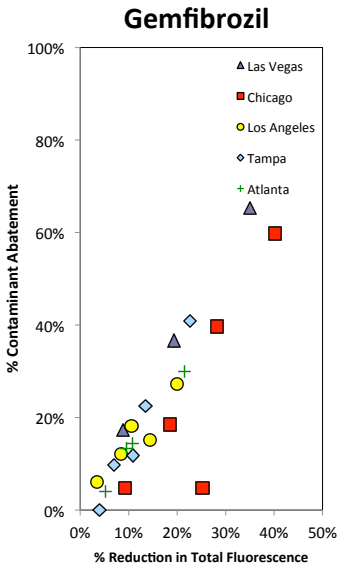

H.

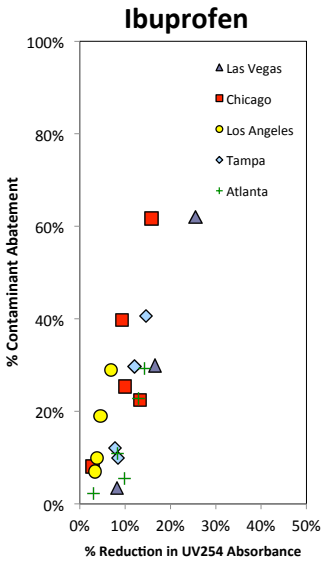

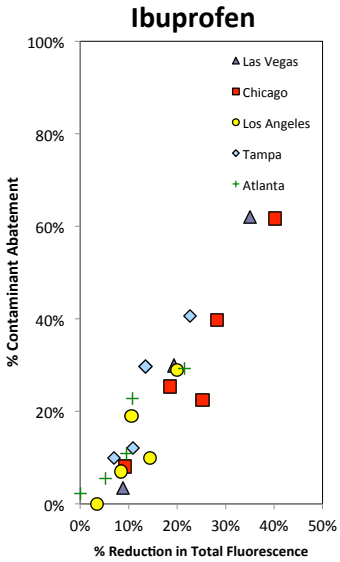

Figure S12. Correlations between target compound oxidation and changes in bulk organic matter differentiated by secondary effluent (left and right) and by study (middle).

I.

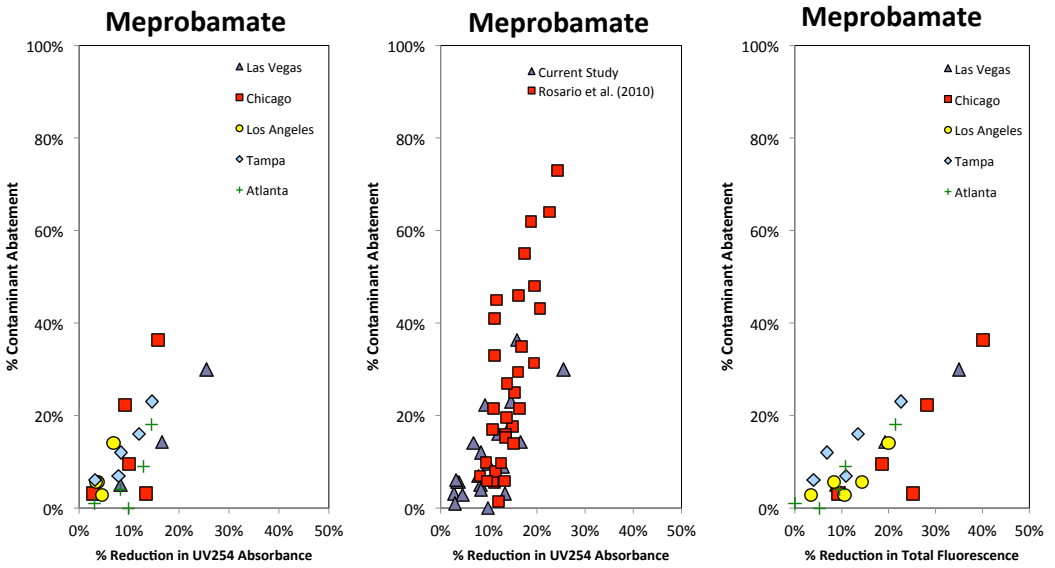

J.

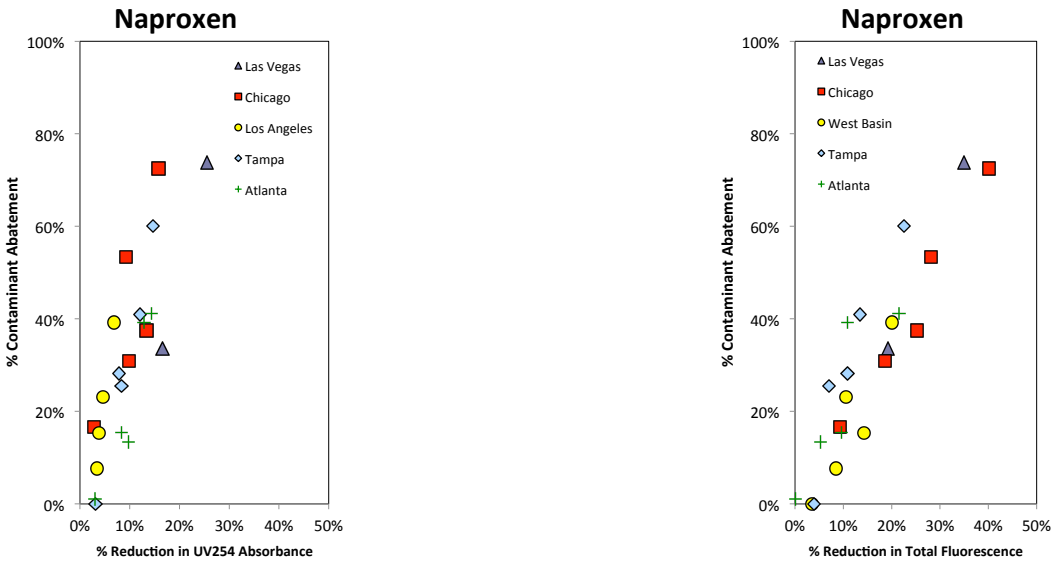

Figure S12. Correlations between target compound oxidation and changes in bulk organic matter differentiated by secondary effluent (left and right) and by study (middle).

K.

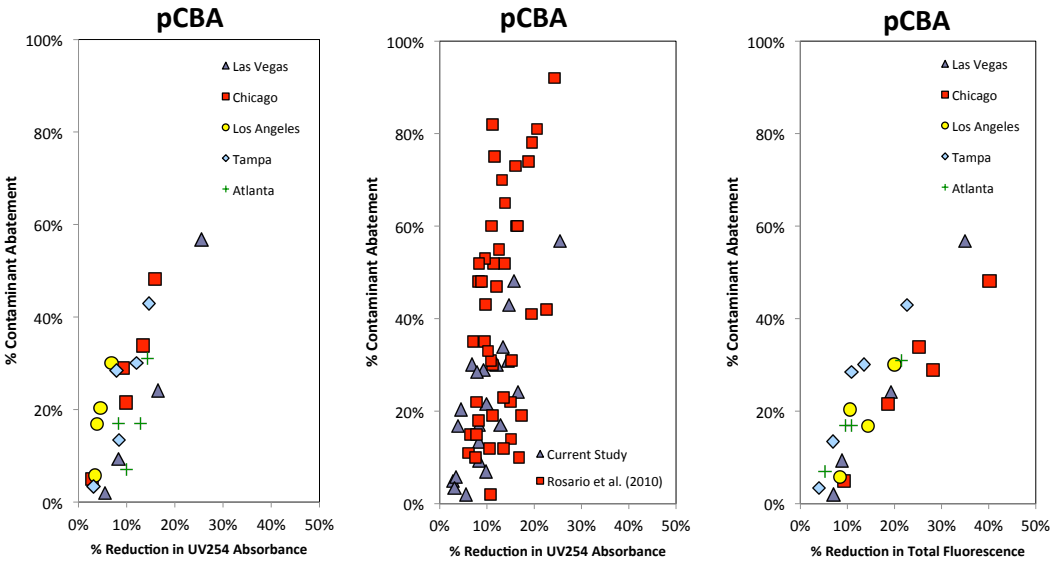

L.

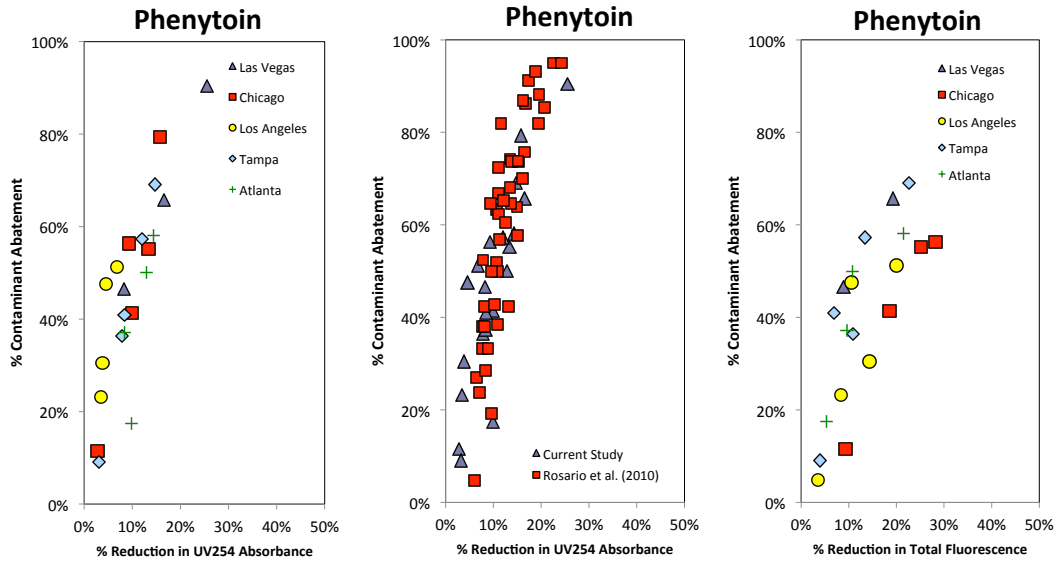

Figure S12. Correlations between target compound oxidation and changes in bulk organic matter differentiated by secondary effluent (left and right) and by study (middle).

M.

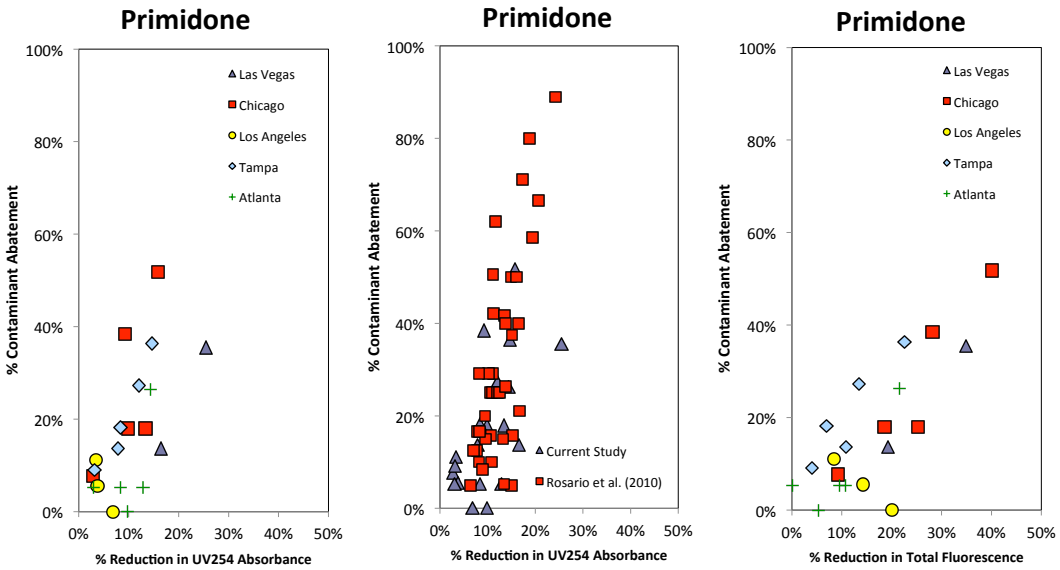

N.

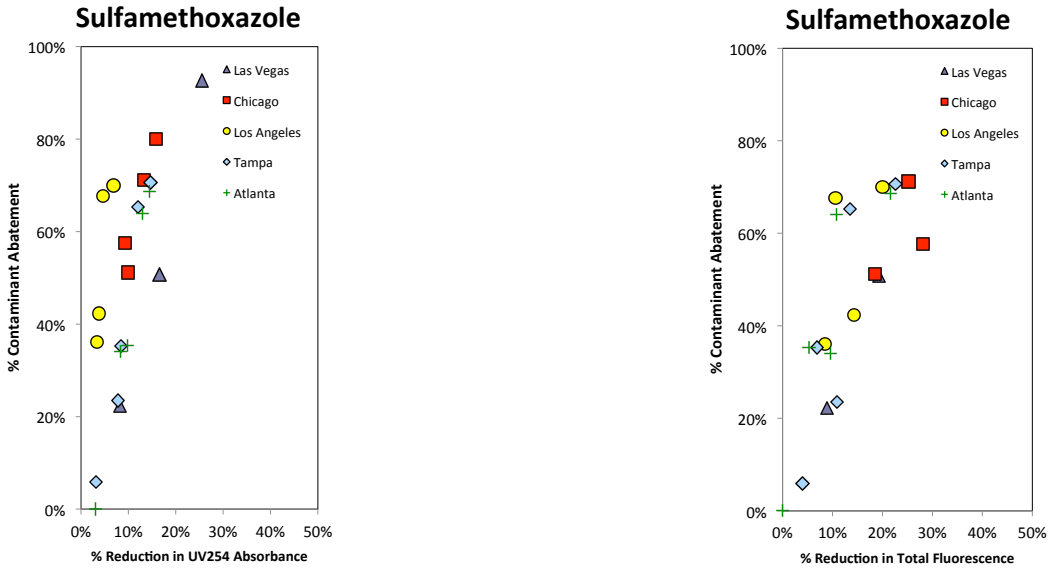

Figure S12. Correlations between target compound oxidation and changes in bulk organic matter differentiated by secondary effluent (left and right) and by study (middle).

O.

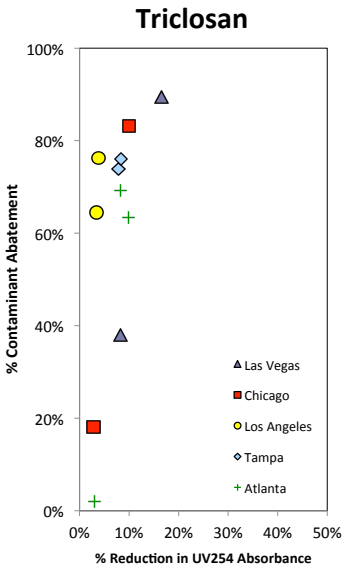

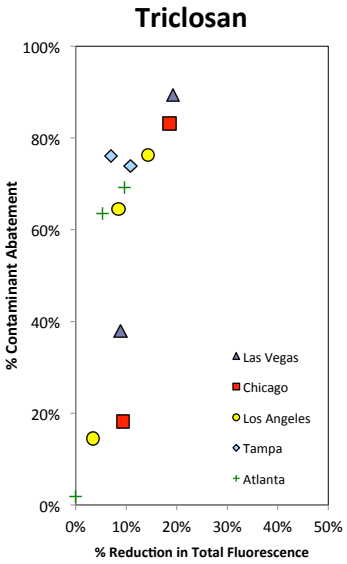

P.